

Physio-Genetic Dissection of Dark-Induced Leaf Senescence and Timing Its Reversal in Barley¹[OPEN]

Ewa Sobieszczuk-Nowicka,^{a,2,3} Tomasz Wrzesiński,^b Agnieszka Bagniewska-Zadworna,^c Szymon Kubala,^d Renata Rucińska-Sobkowiak,^e Władysław Polcyn,^a Lucyna Misztal,^a and Autar K. Mattoo^{f,2,3}

^aDepartment of Plant Physiology, Faculty of Biology, Poznań Adam Mickiewicz University, 61-614 Poznań, Poland

^bEarlham Institute, Norwich Research Park, Norwich, NR4 7UZ, United Kingdom

^cDepartment of General Botany, Faculty of Biology, Adam Mickiewicz University, 61-614 Poznań, Poland

^dInstitute of Biochemistry and Biophysics, Polish Academy of Sciences, 02-106 Warsaw, Poland

^eDepartment of Plant Ecophysiology, Faculty of Biology, Poznań Adam Mickiewicz University, 61-614 Poznań, Poland

^fU.S. Department of Agriculture, Henry A Wallace Beltsville Agricultural Research Center, Sustainable Agricultural Systems Laboratory, Beltsville, Maryland 20705

ORCID IDs: 0000-0002-6603-0582 (E.S.-N.); 0000-0001-9226-7164 (A.K.M.)

Barley crop model was analyzed for early and late events during the dark-induced leaf senescence (DILS) as well as for deciphering critical time limit for reversal of the senescence process. Chlorophyll fluorescence vitality index Rfd was determined as the earliest parameter that correlated well with the cessation of photosynthesis prior to microautophagy symptoms, initiation of DNA degradation, and severalfold increase in the endonuclease *BNUC1*. DILS was found characterized by up-regulation of processes that enable recycling of degraded macromolecules and metabolites, including increased NH_4^+ remobilization, gluconeogenesis, glycolysis, and partial up-regulation of glyoxylate and tricarboxylate acid cycles. The most evident differences in gene medleys between DILS and developmental senescence included hormone-activated signaling pathways, lipid catabolic processes, carbohydrate metabolic processes, low-affinity ammonia remobilization, and RNA methylation. The mega-autophagy symptoms were apparent much later, specifically on day 10 of DILS, when disruption of organelles—nucleus and mitochondria—became evident. Also, during this latter-stage programmed cell death processes, namely, shrinking of the protoplast, tonoplast interruption, and vacuole breakdown, chromatin condensation, more DNA fragmentation, and disintegration of the cell membrane were prominent. Reversal of DILS by re-exposure of the plants from dark to light was possible until but not later than day 7 of dark exposure and was accompanied by regained photosynthesis, increase in chlorophyll, and reversal of Rfd, despite activation of macro-autophagy-related genes.

¹This work was partially supported by the National Science Centre, Poland (project nos. N N303 418236 to E.S.-N. and 2011/01/B/NZ9/00362 to W.P.) and the Department of Plant Physiology, Adam Mickiewicz University Statutory Research Fund (S/P-B/010). A.K.M. was supported by USDA-ARS intramural project no. 8042-21000-142-00D. S.K. acknowledges the financial support of the Polish National Science Centre for the FUGA project for young talented researchers, no. DEC-2015/16/S/NZ2/00042, and the Ministry of Science and Higher Education scholarship, no. 466/STYP/11/2016. The USDA is an Equal Employment Opportunity provider.

²Author for contact: evanna@amu.edu.pl.

³Senior authors.

The author responsible for distribution of materials integral to the findings presented in this article in accordance with the policy described in the Instructions for Authors (www.plantphysiol.org) is: Autar Mattoo (autar.mattoo@ars.usda.gov).

E.S.-N. conceived the original screening and research plan; E.S.-N., T.W., S.K., and R.R.-S., performed the experiments; L.M. provided technical assistance to E.S.-N.; E.S.-N., T.W., A.B.-Z., W.P., and R.R.-S. designed the experiments and analyzed the data; S.K. created the figures; E.S.-N. supervised the research and wrote the first draft with contributions from all the authors; A.K.M. wrote the final version of the manuscript.

[OPEN]Articles can be viewed without a subscription.

www.plantphysiol.org/cgi/doi/10.1104/pp.18.00516

Senescence is a ubiquitous characteristic in the biological world. From an ontogenetic perspective, senescence is now established as a developmental and genetic program acquired during evolution (Wojciechowska et al., 2018). Like in other organisms, senescence in plants is genetically programmed (Nam, 1997; van Doorn and Woltering, 2004; Wojciechowska et al., 2018). In plants, senescence is a prelude to cell (organ) death, and during this process metabolites and macromolecules released are salvaged for utilization by the plant for growth. Generally, senescence occurs prior to programmed cell death (PCD), since symptomatic leaf yellowing can be reversed based on the timing of senescence while PCD is a terminal, irreversible program. It has been suggested that the term “PCD” in plants should be restricted to the specific stage of intrinsic senescence program when it has reached a “point of no return” and leaf yellowing is no longer reversible (Mattoo and Handa, 2003).

Programmed cell death in plants was described as a sequential process that included apoptosis-like necrosis and autophagy (van Doorn et al., 2011). Autophagy under normal growth conditions favors turnover of cellular components for maintaining homeostasis,

while its up-regulation during cell senescence/death leads to irreversible degradation of the cellular components. Plant autophagy processes involve conserved macro-autophagy and microautophagy pathways and a third possibly plant-specific pathway that has been termed mega-autophagy (for review, see Floyd et al., 2015). Microautophagy involves tonoplast invagination resulting in engulfment by intravacuolar vesicles of cytoplasmic and tonoplast components and their uptake into the vacuole (Bassham et al., 2006). Mega-autophagy also leads to degradation of cellular contents by vacuolar enzymes, but it is not involved in the uptake of material into the vacuole. Instead, permeabilization and rupture of the tonoplast releases vacuolar hydrolases into the cytoplasm (Hara-Nishimura et al., 2005; Bollhöner et al., 2012). Macro-autophagy is more related to maintaining normal cellular function; a membranous phagophore is formed that engulfs the “material” to be degraded. As more autophagic cargo is ingested, the phagophore finally closes and forms a double-membrane vesicle called autophagosome, which then transports to the vacuole for degradation of the cargo for recycling (Lamb et al., 2013). Similarly, the orderly progression of leaf senescence involves an efficient recycling process to enable continuance of the vegetative and reproductive development of a plant. During leaf senescence, the enhanced degradation of macromolecules, e.g. proteins, nucleic acids, and sugars, provides material for regulated recycling and reuse by other parts of the plant (Jing et al., 2003).

A majority of the catabolic processes during leaf senescence occur in the chloroplasts, which are marked by decreased photosynthetic activities and, most prominently, the catabolism of chlorophyll (Lutts et al., 1996; Miersch et al., 2000). That leaf senescence process is multifaceted, involving a complex regulatory network, was apparent through studies demonstrating differential and global gene expression during natural and dark-induced senescence in *Arabidopsis thaliana* (Gepstein et al., 2003; Guo et al., 2004; Lin and Wu, 2004; Buchanan-Wollaston et al., 2005). Studies on *Arabidopsis* as a model organism for leaf senescence has revealed several facets of senescence (Lohman et al., 1994; Buchanan-Wollaston et al., 2005). A theoretical model has been put forward about how the capacity to senesce is formulated during leaf development and possibly how internal and external factors are integrated with age to define the timing of senescence (Jing et al., 2003).

There are distinct differences in the senescence program of the plant model *Arabidopsis* and monocot plants. The extensive genomic resources available for *Arabidopsis* make it a very attractive model for the identification and functional analysis of senescence-regulated genes (Buchanan-Wollaston et al., 2003, 2005; Breeze et al., 2011). However, in many plants, such as the pea, removal of the developing flowers and pods significantly extends the life of the leaves (Pic et al., 2002; Buchanan-Wollaston et al., 2003),

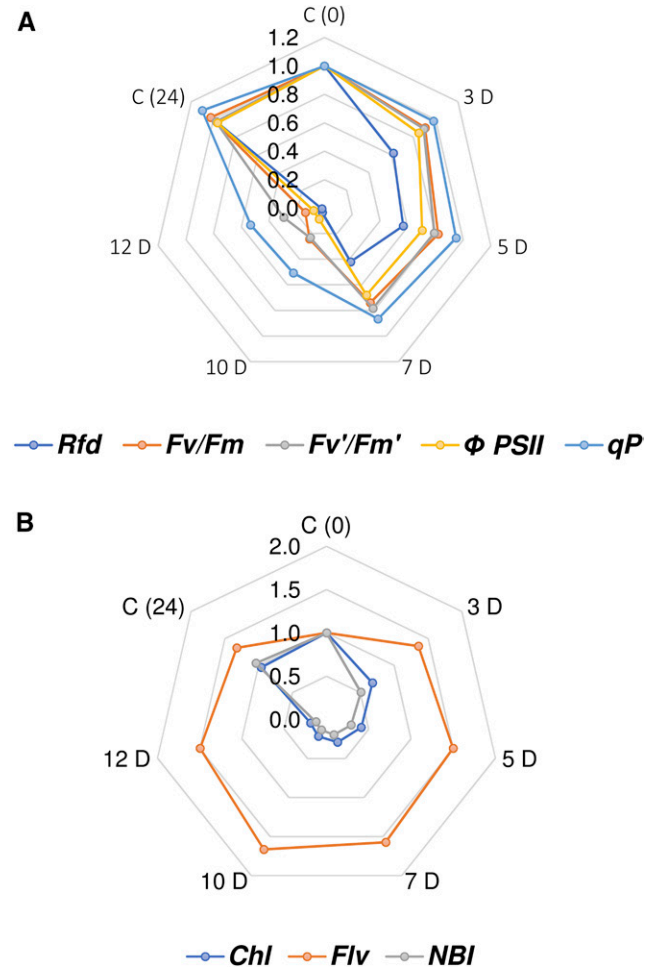


Figure 1. Photosynthetic quantum conversion (A) and leaf nitrogen status (B) parameters in barley leaves undergoing dark-induced senescence. The material for day 0 (0 D) were 7-d-old green barley seedlings not subjected to dark incubation. The senescence process was induced by placing the seedlings in the dark, and primary leaf material was collected for measurements on days 3, 5, 7, 10, and 12. Chlorophyll fluorescence induction kinetics parameters such as F_v/F_m , F_v'/F_m' , qP , NPQ, $\Phi PSII$, Rfd, and plant nitrogen status (Chl, Flv, and NBI indexes) were then measured. Rfd, Chl fluorescence decrease ratio, the survival rate of PSII; F_v/F_m , maximum quantum yield of PSII in the dark-adapted state; F_v'/F_m' , maximum quantum yield of PSII in the light-adapted state; $\Phi PSII$, effective quantum yield of PSII electron transport; qP , photochemical quenching of Chl fluorescence; NPQ, nonphotochemical quenching of Chl fluorescence; Chl, leaf chlorophyll concentration; Flv, leaf flavonoid concentration; NBI, nitrogen balance index. The data are presented as fold changes relative to day 0. The differences in the measured parameters were analyzed for statistical significance using one-way ANOVA and the Tukey-Kramer Multiple Comparison Test ($n = 15$ for photosynthetic quantum conversion and leaf nitrogen status parameters and $n = 6$, $P < 0.01$). The same letters indicate non-significant differences between means (Supplemental Table S1).

while in *Arabidopsis*, the development of male sterile mutants or removal of developing bolts does not result in extension of the life of individual leaves (Hensel et al., 1993; Buchanan-Wollaston et al., 2003). Moreover,

only limited information about senescence-associated genes (SAGs) is available for crop plants, including maize (*Zea mays*; Smart et al., 1995), rice (*Oryza sativa*; Lee et al., 2001), wheat (*Triticum aestivum*; Uauy et al., 2006) and barley (*Hordeum vulgare*; Kleber-Janke and Krupinska, 1997; Jukanti et al., 2008; Christiansen and Gregersen, 2014; Avila-Ospina et al., 2015; Springer et al., 2015; Wehner et al., 2015), unlike for Arabidopsis. Because of these differences, cereal leaves have been used as an additional model for studying leaf development and senescence (Sobieszczyk-Nowicka et al., 2009, 2015, 2016; Legocka et al., 2015).

Senescence in cereals is mostly regulated at the level of the individual leaf. Nutrients from the older leaves are thus mobilized initially for the younger leaves and eventually for the flag leaf, contributing, therefore, to photoassimilates required for grain development. As opposed to the leaves of dicotyledonous species, cereal leaves have a basal meristem and a leaf tip consisting of older cells, while the younger cells are concentrated at the leaf base. Such a cellular organization makes studies on senescence progression pertinent and clear (Gregersen et al., 2008). However, the lack of coordinated development of the cells within an individual leaf makes studies on leaf senescence complex. Therefore, artificially induced senescence that directs a synchronous process, such as dark-induced senescence, has become a more commonly used technique in such studies (Buchanan-Wollaston et al., 2005).

Dark-induced leaf senescence (DILS) is an extreme example of shading that induces leaf senescence similar to that observed during normal plant development. Also, the DILS model eliminates the confounding factors that overlap with developmental senescence, such as bolting or flowering. It has been argued that the primary reason for cell death is a stress response, with the death of the organ being necessary or advantageous to the rest of the plant, even without nutrient recycling (Thomas, 2013). Barley was one of the first cereals domesticated in the Fertile Crescent, and today, it is the fourth most important cereal crop after wheat, maize, and rice. Worldwide, barley is mainly used for animal feed and malting. Both biotic and abiotic stresses (heat, salinity, drought, and N deficit) significantly reduce barley yield in many parts of the world (Wehner et al., 2015). In the juvenile stages of wheat, from sowing to tillering, environmental stresses can severely affect its development and potential yield. Such pre- and postharvest losses can amount to as much as 30% of the crop (El Hafid et al., 1998; Gepstein and Glick, 2013).

This study utilized DILS as a model to examine early and late events in barley leaf senescence. Specifically, we present transcriptomic, cytological, and physiological data that reveal events in DILS, differences from developmental senescence, time limit for dark-to-light transition for reversal of the senescence process, and progression of senescence through autophagy into the PCD phase.

RESULTS

Photosynthetic Quantum Conversion and Leaf Nitrogen Status in Senescing Barley Leaves

Chlorophyll *a* fluorescence kinetics and leaf nitrogen status in green and senescing barley leaves were determined from days 0 to 12 after exposure to total darkness. Effective quantum yield of PSII electron transport (Φ PSII) gradually decreased in two consecutive steps until day 7 and was then accompanied with a sharp decrease at day 10 (Fig. 1; Supplemental Table S1). Chl fluorescence decrease ratio, called the vitality index (Rfd) changed even more dramatically, with the decline taking place as early as days 3 and 5. A small reduction of maximum quantum yield of PSII in the dark-adapted state (F_v/F_m), maximum quantum yield of PSII in the light-adapted state (F_v'/F_m') and photochemical quenching of Chl fluorescence (qP) values was registered at day 7, but much more dramatic reduction of these parameters occurred thereafter (Fig. 1; Supplemental Table S1). This was accompanied by a severe loss of chlorophyll, indicator of nitrogen-compound remobilization, and an increase in flavonoid (Flv) content—the hallmark of reduced carbon use. Changes in these parameters caused a decrease in nitrogen balance index (NBI) to a level almost three times lower than that in the control at day 7, and by days 10 and 12, it was four times lower. Based on this chronological sequence of leaf senescence stages, for further experiments, we chose leaves that were dark incubated for 0 (control), 3, 7, and 10 d.

Senescence Symptoms in Parenchyma Cells

Chloroplast Cytology

Visible morphological changes that were apparent in leaves during senescence are shown in Figure 2. The progression of leaf senescence was reflected by the gradual changes in color from green to yellow; on day 7, traces of visible necrosis in the apical part of the leaf became noticeable, which finally were apparent throughout the leaf by day 10 of dark exposure (Fig. 2A). The senescence-dependent decrease in chlorophyll correlated with gradual loss of its autofluorescence (Fig. 2B).

Detailed cytological analyses were performed on chloroplasts and nuclei of leaf parenchyma cells, since significant changes in their ultrastructure were noticed within the first 24 h of exposure to darkness (Fig. 2, C and D). Chloroplasts from the “control” leaves showed typical structure with visible inner and outer chloroplast membranes together with the thylakoid system clearly visible (Fig. 2C). On day 3 of dark-induced senescence, chloroplast shape changed from lenticular to more spherical, and, in most cases, thylakoids had swollen (Fig. 2D). On day 7, numerous plastoglobuli were present (Fig. 2, C and D), which seem to have

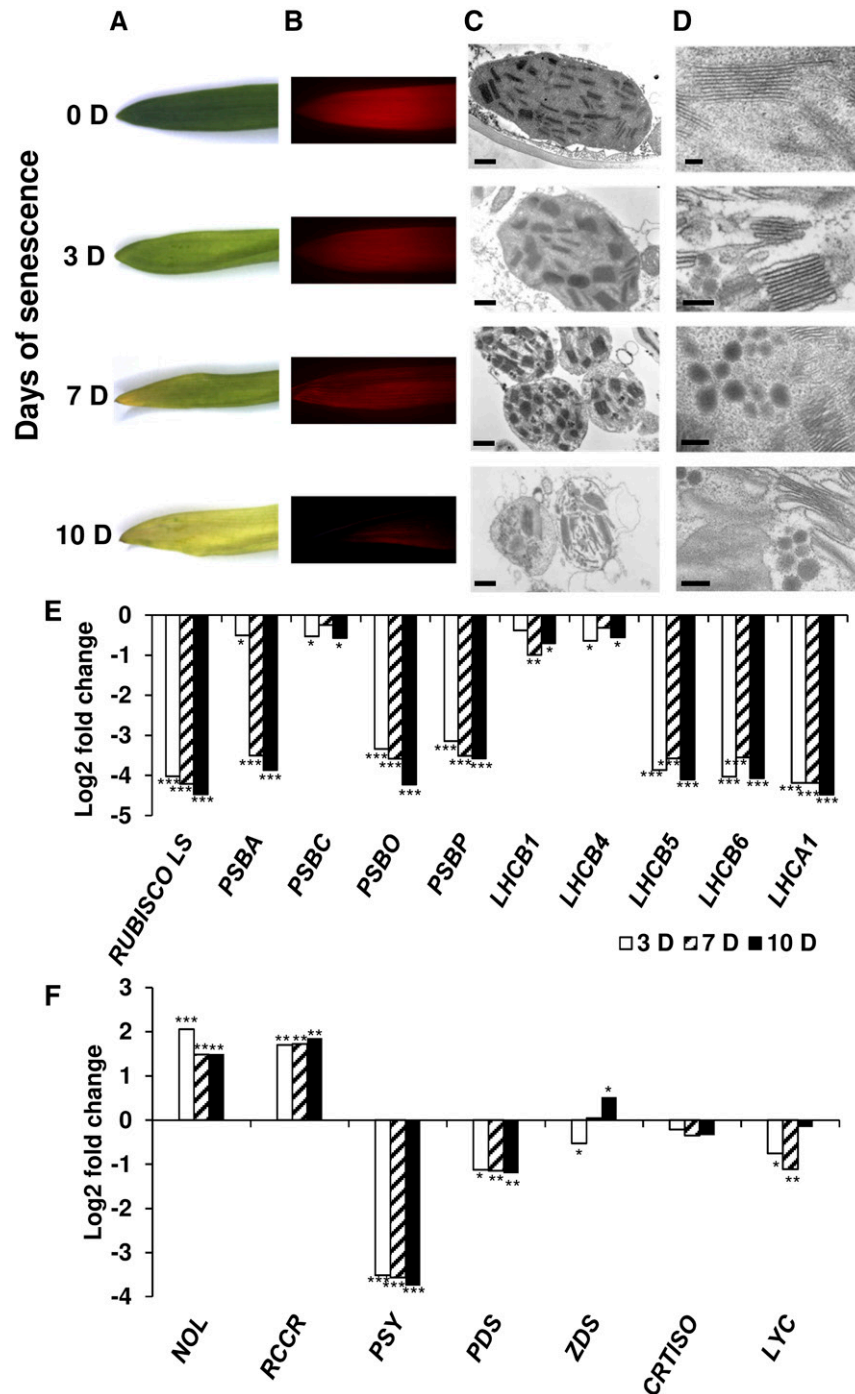


Figure 2. Leaf morphology (A and B; autofluorescence) and ultrastructure of chloroplast (C) and thylakoid (D) and the time course of expression of genes involved in photosynthesis, chlorophyll, and carotenoid metabolism (E and F) in barley leaves undergoing dark-induced leaf senescence. Primary barley leaves from plants subjected to 3, 7, and 10 d of dark incubation were used to determine leaf morphology and for genomic and cytological characterization. The control material for day 0 (0 D) was 7-d-old green barley seedlings not subjected to dark incubation. *Rubisco LS*; *PSBA*, PSII reaction center protein A; *PSBC*, PSII reaction center protein C; *PSBO*, PSII manganese-stabilizing protein; *PSBP*, PSII subunit P; *LHCB1*, light-harvesting chlorophyll *a/b*-binding protein; *LHCB4*, light-harvesting complex PSII; *LHCB5*, light-harvesting complex of PSII subunit 5; *LHCB6*, light-harvesting complex PSII subunit 6; *LHCA1*, PSI light-harvesting complex gene1; *NOL*, *NYC1-LIKE* (chlorophyll *b* reductase); *RCCR*, red chlorophyll catabolite reductase; *PSY*, phytoene synthase; *PDS*, phytoene desaturase; *ZDS*, zeta-carotene desaturase, and *CRTISO*, carotenoid isomerase; *LYC*, lycopene cyclase. The gene expression data are from the time-course experiment performed with the Agilent oligonucleotide microarray (Zmienko et al., 2015a, 2015b). The data are presented as log₂ FCs relative to day 0. Differential gene expression was evaluated with Bayesian linear modeling (R/Bioconductor, limma

pushed thylakoids to the side. By day 10, dark-induced senescence symptomology of the chloroplast ultrastructure had progressed to a state with increased number of plastoglobules, largely swollen thylakoids, and breakdown of chloroplasts (Fig. 2, C and D).

Nucleus Cytology and nDNA Fragmentation

Nuclei from the control material were true-to-type, usually with scattered chromatin, a few more condensed heterochromatin areas and one compact nucleolus (Fig. 3A; 0 d). On day 3 of dark-induced senescence, the ultrastructure of the nucleus did not change much, while chromatin was condensed. Subsequently, with prolonged senescence, the shape of nuclei became irregular (Fig. 3A). Senescence-mediated changes in the structure/shape of the nucleus were accompanied by nuclear DNA fragmentation. The comets in samples from days 0, 3, 7, and 10 of senescence are shown in Figure 3B. The head corresponds to the amount of DNA remaining with the nuclear matrix, whereas the tail represents the DNA fragments migrating from the nucleus. For the control variant and day 3-senescent leaves, the images of the isolated nucleus contain a typical comet with a head and a tail (Fig. 3B). By day 7 and 10, the typical comet was replaced by a large headed comet (a halo of granular DNA and a hazy outer boundary) and a short tail (Fig. 3B). The comet for barley is not a typical “head and tail” one. Interestingly, a comet assay of the nucleus of an apoptotic cell showed a halo of granular DNA and a hazy outer boundary, likely a result of nucleosome-sized DNA diffusion into agarose (Singh, 2000). Our experimental approach allowed us to observe both, (1) moderate DNA fragmentation and (2) more global DNA damage typical in dying cells. DNA migration was visible in variants where moderate DNA damage led to the formation of classic DNA comets. The percentage of DNA tail was measured from the center of the head to the end of the tail (Fig. 3C). Our data indicated that the amount of cleaved DNA fragments liberated from damaged nuclei of barley leaves was prominent early during exposure of barley leaves to darkness. On day 3 of senescence, % of the DNA tail was lower than that in the control, but the lowest % of DNA tail was observed in day 7 and day 10 samples (Fig. 3C).

Protein and Gene Indicators

The changes in chloroplast ultrastructure and stability of the nucleus during dark-induced barley leaf senescence prompted us to assess the levels of marker proteins/genes relevant to chloroplast biochemistry. First, major chloroplast proteins—the soluble Rubisco (Grabsztunowicz et al., 2015) and membrane-associated

PSII reaction center D1 protein (Mattoo et al., 1989) were isolated from barley leaf chloroplasts from day 0 to day 12 of dark-induced senescence, and the protein samples were gel fractionated and immunoblotted. Rubisco protein level decreased significantly from the start of the senescence to about 60% and 21% of the control level by days 7 and 10 of senescence, respectively (Supplemental Fig. S1A). Interestingly and in contrast, the level of the D1 protein did not change up to 5 d of senescence, decreasing only by 7% on day 7 and 23% on day 10 (Supplemental Fig. S1B). At the gene-transcript levels, we utilized our generated microarray data to evaluate select barley genes for expression in DILS (Figs. 2–4), the notable decrease in Rubisco protein levels seen above was found associated with down-regulation of its gene transcripts (Fig. 2E). In the case of chloroplast-encoded *PSBA* gene, which encodes the D1 protein, there was clear disconnect between the stability of D1 protein during barley leaf senescence seen above and the expression of *PSBA* gene transcript levels. *PSBA* gene transcripts were ~11- and ~14-fold lower in samples from days 7 and 10 of dark-induced senescence, respectively (Fig. 2E; *PSBA*), which indicates that the D1 protein is under posttranscriptional control.

The major impact on the gene expression of the two important proteins associated with chloroplasts, Rubisco, and D1, prompted us to quantify the transcript levels of other protein genes associated with leaf senescence. Generally, we observed down-regulation by ~10-fold on day 3 to ~20-fold on day 10 of the following photosynthesis-related genes in response to senescence: *Rubisco LS*; PSII manganese-stabilizing protein (*PSBO*), 33-kD protein of the oxygen evolving complex, light-harvesting complex of PSII subunit 5 (*LHCB5*), CP26 chlorophyll a/b-binding protein of plant PSII, light-harvesting complex of photosystem II subunit 6 (*LHCB 6*), CP24 chlorophyll a/b-binding protein of plant PSII, and the light-harvesting protein *LHCA1*. *LHCA1* is one of the four main and highly conserved types of chlorophyll a/b-binding proteins (*LHCA1–4*) of the light-harvesting antenna of PSI (Fig. 2E). In contrast, change in pigmentation of barley leaves undergoing dark-induced senescence was found to be accompanied by up-regulation of genes involved in chlorophyll degradation. Chlorophyll *b* reductase involved in the degradation of chlorophyll *b* (*NOL*) increased by ~4-fold and red chlorophyll catabolite reductase increased by ~3-fold. Genes involved in carotenoid biosynthesis were mostly down-regulated during DILS, including phytoene synthase, phytoene desaturase, carotenoid isomerase, and lycopene cyclase, with the exception of zeta-carotene desaturase—which is involved in the biosynthesis of both carotenes and xanthophylls and whose expression decreased

Figure 2. (Continued.)

package) with Benjamini and Hochberg's correction of the false discovery rate. The adjusted *P* values are marked as **P* < 0.05, ***P* < 0.005, and ****P* < 0.0005. Bars, 500 nm (column C); 50 nm day 0, 100 nm days 3, 7, and 10 (column D).

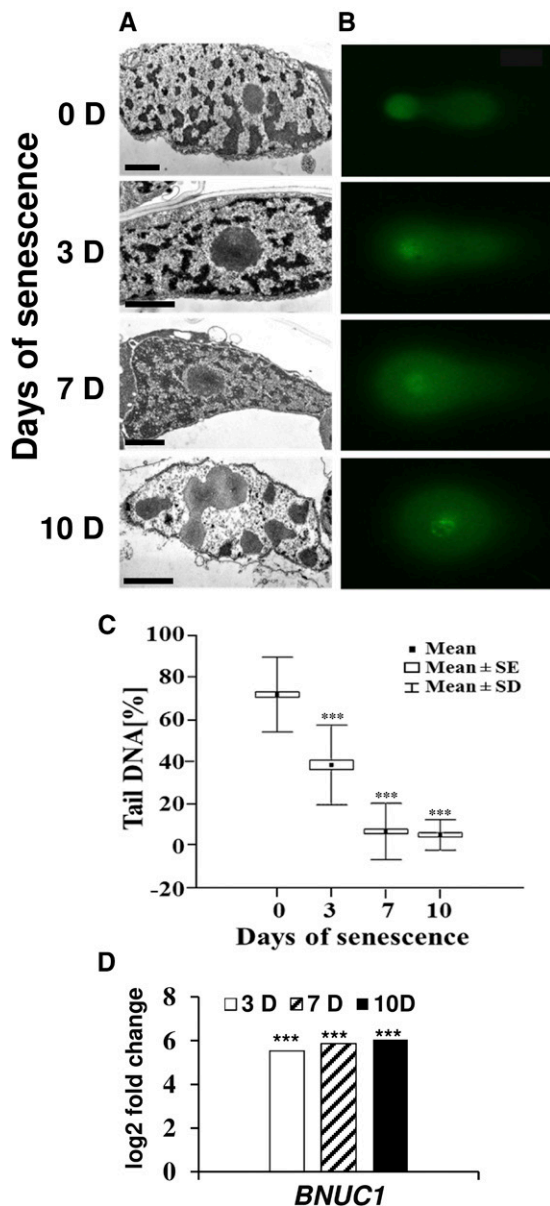


Figure 3. Nucleus ultrastructure (A), comet images after alkaline single-cell gel electrophoresis followed by SYBR green staining (B), box plots of the % of DNA tail (C), and time course of endonuclease *BNUC1* expression (D) in barley leaves during dark-induced leaf senescence. Plant material (primary barley leaf) for capturing cytological analysis and nuclei isolation for comet assay was the same as described in the legend to Fig. 2. The control material for day 0 (0 D) was 7-d-old green barley seedlings not subjected to dark incubation. Box plots represent data on 150 scored comets from each treatment. Asterisks denote significant differences from the control (Kruskal-Wallis ANOVA test; $P < 0.001$). The gene expression data are from the time-course experiment performed with the Agilent oligonucleotide microarray. The data are presented as log₂ FCs relative to day 0. Differential gene expression was evaluated with Bayesian linear modeling (R/Bioconductor, limmapackage) with Benjamini and Hochberg's correction of the false discovery rate. The adjusted P values are marked with $***P < 0.0005$. Bars, 1 μ m.

~1.5-fold at day 3 of senescence but increased ~1.5-fold on day 10 (Fig. 2F).

The *BNUC1* gene encodes an endonuclease generally associated with senescence (Sakamoto and Takami, 2014). It is a marker of DNA degradation in senescence. We quantified the expression of this gene in DILS on days 0, 3, 7, and 10 (Fig. 3D). DILS was associated with high induction of *Bnucl1* gene expression, increasing from 46-fold change on day 3, 57-fold on day 7, and 65-fold on day 10 of DILS as compared to day 0 samples (Fig. 3D).

Autophagy Symptoms: Cytology and Gene Indicators

Ultrastructural analysis of senescing parenchyma cells showed the control cells with a large centrally located vacuole, and the cytoplasm located along the cell wall. The numerous lenticular chloroplasts in the cytoplasm, nucleus, and mitochondria were thus located peripherally (Fig. 4A). During the initial senescence period, day 3 of darkness, tonoplast invagination, presence of small cytoplasmic fragments near or connected with tonoplast and vacuoles (Fig. 4B, arrows) and shrunken protoplasts were apparent. On day 7 of senescence, a few cells showed discontinuity of the cell membrane, while by day 10, tonoplast apparently ruptured (Fig. 4, A and B). Consequently, all the organelles underwent gradual disintegration and were localized to the central part of the cell. The cell membrane increasingly loosened and, consequently, the intracellular compartmentation was lost. Cell death during senescence was distinguished by fast-occurring changes in the chloroplasts (Fig. 4, A and B), whereas the nucleus and mitochondria were relatively more stable, and their degradation occurred only after the final lytic stage following vacuole tonoplast rupture. In the later stages of cell death, it was not possible to accurately distinguish specific organelles. However, the shrinking of the protoplast and deformation of the cell wall were clearly observed on the micrographs (Fig. 4A).

Autophagy was apparent during ultrastructural observations of senescing parenchyma cells seen as small autophagic bodies inside vacuoles, autophagosomes presence in protoplasts, and during tonoplast rupture. Therefore, we quantified a set of autophagy-related genes (*ATGs*) and genes involved in *ATG*-independent alternative cell degradation pathways—senescence-associated vacuole formation (*VPEs*, vacuolar-processing enzymes). Clearly, most of the *ATGs* were expressed at high levels during progression of barley leaf senescence (Fig. 4C). Also, among the two vacuolar-processing enzymes quantified, α *VPE* was more highly upregulated, from 1.8-fold on day 3 to 3.1-fold for day 10 of DILS; *VPE2c* was less so, with its level increasing 1.2-fold on day 3, 1.75-fold on day 7 and 1.15-fold on day 10 (Fig. 4C). Relative to the expression of these genes, that of the known senescence-activated marker gene Cys protease (*SAG12*) was minimally induced (1.03- to 1.6-fold increase).

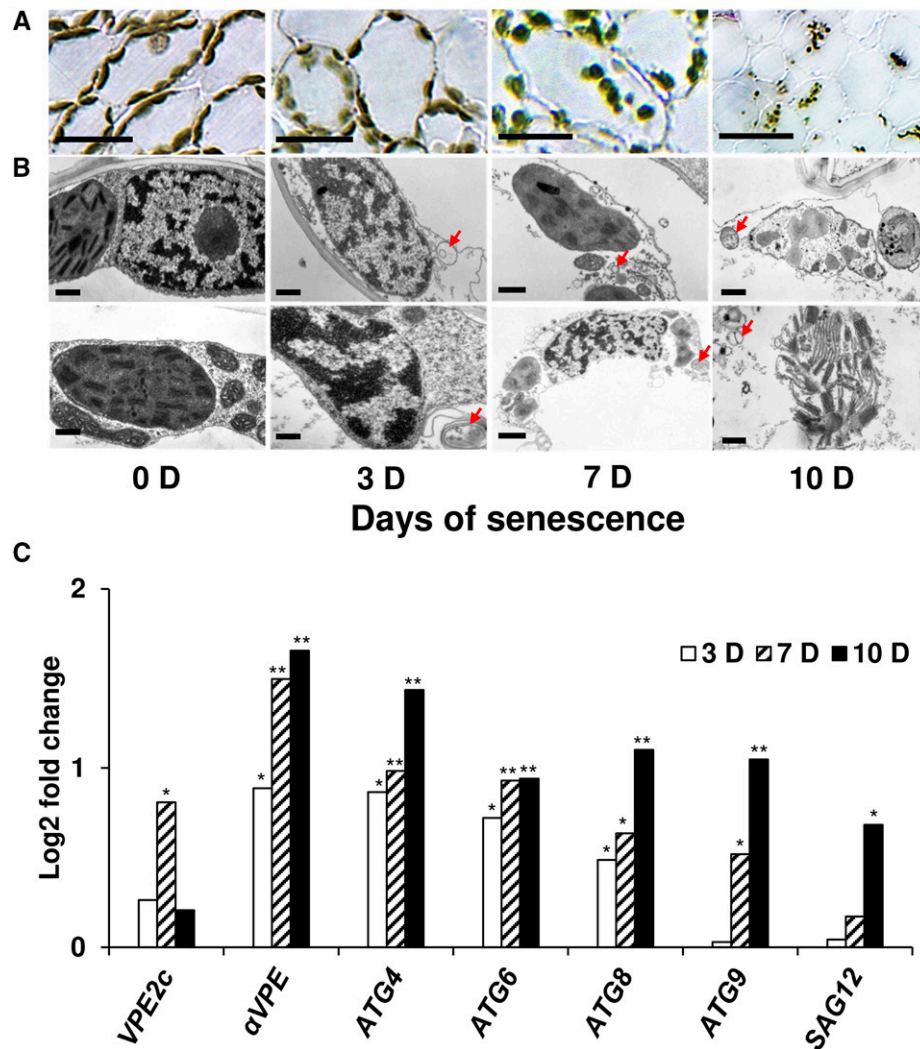


Figure 4. Autophagy symptoms of dark-induced senescing parenchyma barley cells. Leaf anatomy (A), ultrastructure (B), and time course of expression of genes involved in autophagy (C) in barley leaves during dark-induced senescence. Plant leaf material and control day 0 (0 D) samples were the same as described in the legend to Fig. 2. The gene expression data for *VPE2c* (vacuolar-processing enzyme), α *VPE* (vacuolar-processing enzyme), *ATGs* (autophagy-related genes 4, 6, 8, 9), and *SAG12* (senescence-associated gene, Cys protease) are from the time-course experiment performed with the Agilent oligonucleotide microarray. The data are presented as log₂ FCs relative to day 0. Differential gene expression was evaluated with Bayesian linear modeling (R/Bioconductor, limmapackage) with Benjamini and Hochberg's correction of the false discovery rate. *P* values are marked with **P* < 0.05 and ***P* < 0.005. Bars, 25 μ m days 0 and 3, 40 μ m day 7, and 10 μ m day 10 (A). Bars, 200 nm days 0 and 3; 500 nm days 7 and 10 (top row of B); Bars, 200 nm days 0, 3, 7, and 10 (bottom row of B). Arrows indicate vesicles with electron-dense and lucent cargoes and vacuoles that contained several autophagic-like bodies with cytoplasm-derived structures.

Transcriptome of Dark-Induced Leaf Senescence

The above data demonstrate that barley leaf senescence induced by long-term dark incubation is associated with a number of gene medleys associated with chloroplast/photosynthesis function, autophagy, nitrogen, and carbon assimilation, and organelle disintegration. Therefore, to obtain a more global picture of the barley DILS, we studied differential gene expression during this process by employing Barley Gene Expression Microarrays, 4 \times 44K (Agilent) and generating time-course profiles using samples incubated

in the dark for 0, 3, 7 and 10 d. Out of the 43,603 unique oligonucleotide probes present on the microarray, 3,014 showed differential gene expression, with moderated F-statistic *P* value < 0.0005, utilizing Benjamini and Hochberg's method (Benjamini and Hochberg, 1995) to limit the false discovery rate. Although we cannot exclude that a single gene may, in fact, be represented by multiple probes on the Barley Gene Expression Microarrays, we considered the assumption that the number of differentially regulated genes equals the number of probes. As many as 70%

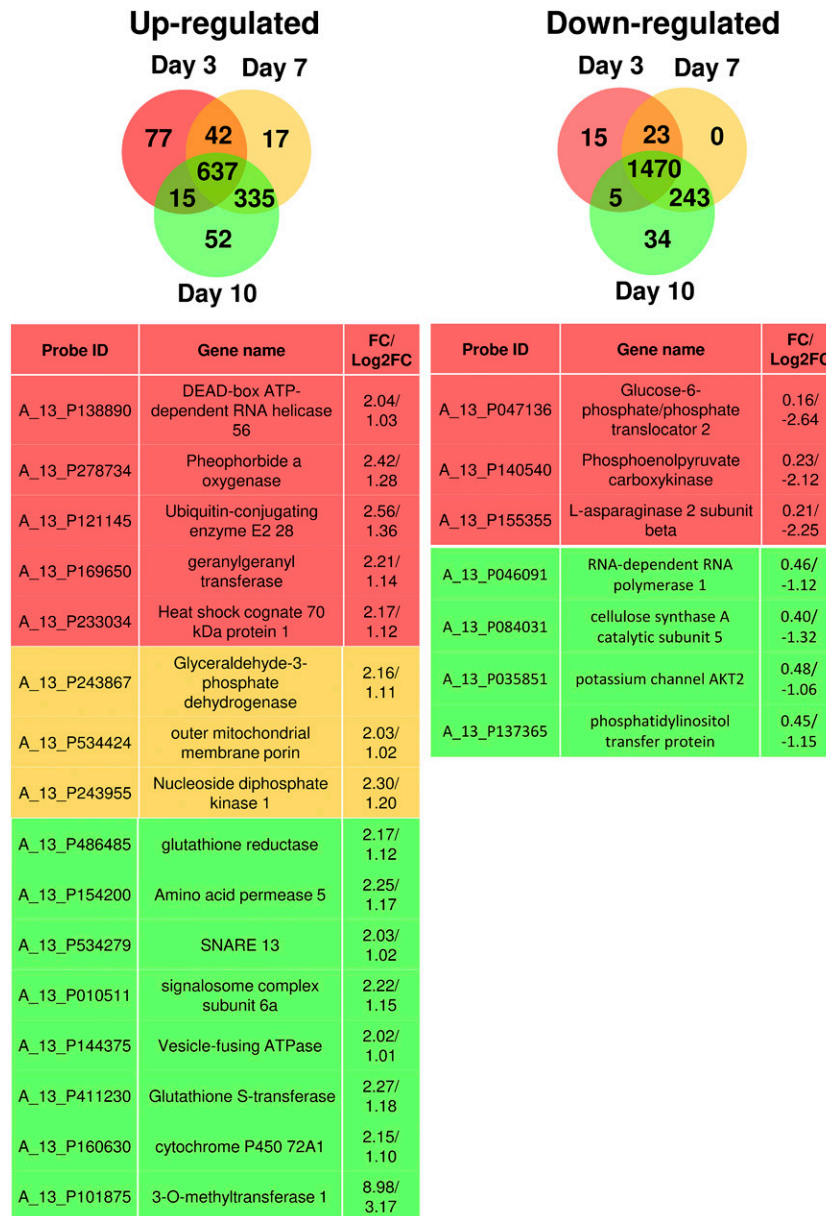


Figure 5. Changes in gene expression on days 3, 7, and 10 during dark-induced senescence of barley leaves. Venn diagrams present genes differentially expressed (F-statistics, $P < 0.0005$ [after applying Benjamini and Hochberg's method to control the false discovery rate]) and displaying at least 2-fold expression change (\log_2 FC = 1 or -1) at a given time point. Genes whose expression was affected only at a particular time point are presented within the rectangles. The gene expression data are from the time-course experiment described in the legend to Fig. 3. This figure was generated from data presented in Supplemental Tables S2 and S3.

of differentially regulated genes underwent at least a 2 fold change in expression at the analyzed time points (days 3, 7, and 10). In all but two of the above cases, 637 genes were consistently up-regulated while 1,470 genes were consistently down-regulated. For a subset of such genes (19% up-regulated and 16% down-regulated, respectively), the response was also time dependent: the induction or repression being ≥ 2 times higher at day 10 than at day 3 (Fig. 5; Supplemental Tables S2

and S3). Also, about 181 candidate genes had less than 20% change in expression at the three analyzed time points and displayed very low signal intensity variation across individual hybridizations.

Genes whose expression was altered at a specific time point are summarized in Figure 5 and Supplemental Table S3. In particular, among the 77 genes up-regulated exclusively on day 3 of DILS as compared to the control (\log_2 fold change [FC] = 1.133–1.476)

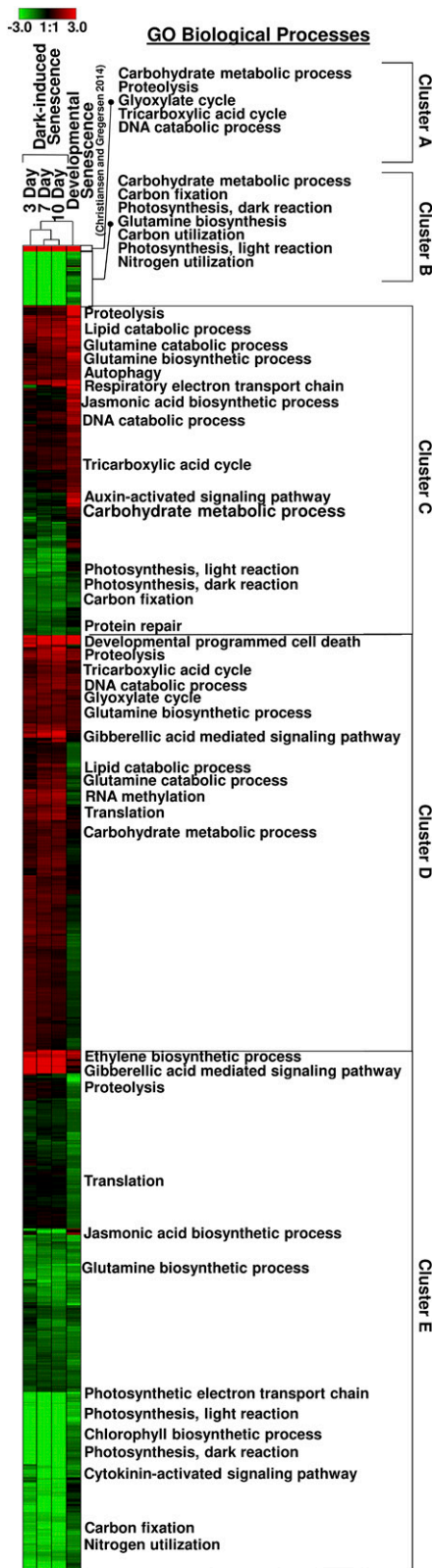


Figure 6. Hierarchical clustering of genes involved in dark-induced (DILS) versus developmental leaf senescence (DLS) in barley. A heat map was used to depict \log_2 FC of gene expression levels (green and red colors represent down- and up-regulated genes, respectively)

include aspartyl protease, geranylgeranyl transferase, DEAD-box ATP-dependent RNA helicase, pheophorbide *a* oxygenase, heat-shock cognate 70-kDa protein, and ubiquitin-conjugating enzyme (Fig. 5; Supplemental Table S3). Simultaneously, genes encoding Glu dehydrogenase, phosphoenolpyruvate carboxykinase, and Glc-6-phosphate dehydrogenase were specifically down-regulated on day 3 of DILS (\log_2 FC = -1.519 to -2.61). Genes encoding outer mitochondrial membrane porin, conserved oligomeric Golgi complex component, glyceraldehyde-3-phosphate dehydrogenase, cochaperone protein SBA, and nucleoside diphosphate kinase had higher expression on day 7 as compared to the control (\log_2 FC = 1.025 – 1.206). Genes that were specifically up-regulated on day 10 included signalosome complex subunit, vesicle-fusing ATPase, SNARE complex, glutathione reductase, amino acid permease, cytochrome P450, glutathione *S*-transferase, and *O*-methyltransferase family 2, with \log_2 FC between 1.019 and 3.168 . At the same time point (day 10), 34 genes were specifically down-regulated, with the \log_2 FC in the range of -1.042 to -1.938 , including genes for potassium channel protein, RNA-dependent RNA polymerase, phosphatidylinositol transfer protein, cellulose synthase, and glycosyl hydrolase (\log_2 FC = -1.938 , adjusted *P* value = 1.1×10^{-5}). It was particularly apparent that on day 7 of dark exposure, no genes were exclusively down-regulated.

Five distinct gene groups could be classified using hierarchical clustering, depicting GO biological processes (Fig. 6; Supplemental Table S4). Cluster A includes genes, such as glycosyl hydrolase family (carbohydrate metabolism), isocitrate lyase (glyoxalate/Krebs cycle), PA3 nuclease (DNA catabolism) and vignain precursor (proteolysis), which were more highly up-regulated in DILS samples from day 3 through day 10 than in the control (increase in the expression was more or less 60 times compared to the day 0 sample). Cluster B comprises down-regulated genes during DILS related to carbohydrate metabolism (Fru-bisphosphate aldolase isozyme, Fru-1,6-bisphosphatase, and Fru-bisphosphate aldolase isozyme), photosynthesis (ferredoxin-NADP reductase, chloroplast precursor, chlorophyll *a/b*-binding protein, glyceraldehyde-3-phosphate dehydrogenase), C and N utilization (carbonic anhydrase, chloroplast precursor, cinnamoyl-CoA reductase), and Gln biosynthesis (Gln synthetase, catalytic domain-containing protein). The cinnamoyl-CoA reductase gene expression decreased 10-fold on day 3 and 38-fold at day 10 of DILS. The cluster C group includes genes involved in proteolysis (pyrrolidone-carboxylate peptidase and ICE-like protease p20 domain-containing

between DILS samples (days 3–10) and controls (day 0) as well as DLS in comparison to nonsenescent samples (Christiansen and Gregersen, 2014). Genes belonging to a cluster (presented on the right-hand side of the heat map) were annotated with GO terms. All the original data from which this figure was generated involved utilizing 22 thousand probes and data obtained are given in Supplemental Table S4.

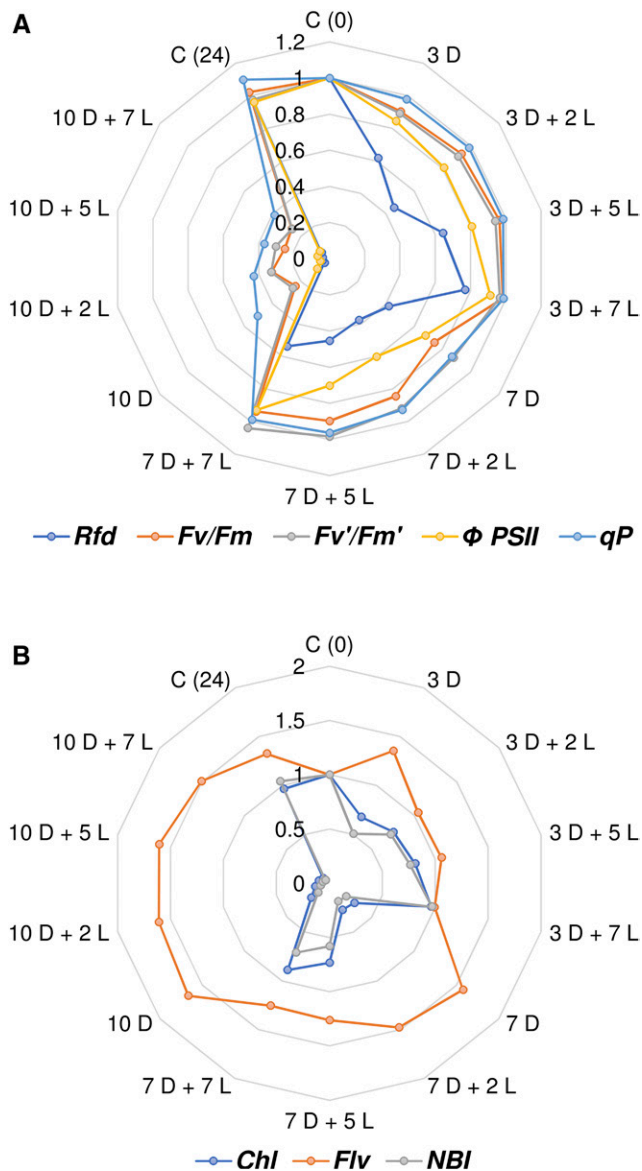


Figure 7. Photosynthetic quantum conversion (A) and leaf nitrogen status (B) parameters in barley leaves undergoing dark-induced senescence and upon regreening. Day 0 material was from 7-d-old green barley seedlings not subjected to dark incubation. The senescence process was induced by placing the seedlings in the dark (D) for 3, 5, 7, and 10 d. Leaves in the dark incubation were moved at indicated times and re-exposed to light (L) for a period of 2, 5, and 7 d. The control sample (C) for the regreening system was the one not exposed to dark (D). *Rfd*, Chl fluorescence decrease ratio, the survival rate of PSII; F_v/F_m , maximum quantum yield of PSII in the dark-adapted state; F_v'/F_m' , maximum quantum yield of PSII in the light-adapted state; Φ_{PSII} , effective quantum yield of PSII electron transport; *qP*, photochemical quenching of Chl fluorescence; NPQ, nonphotochemical quenching of Chl fluorescence; Chl, leaf chlorophyll concentration; Flv, leaf flavonoid concentration; NBI, nitrogen balance index. The data are presented as fold changes relative to day 0. The differences in the measured parameters were analyzed for statistical significance using one-way ANOVA and the Tukey-Kramer multiple comparison test ($n = 15$ for photosynthetic quantum conversion and leaf nitrogen status parameters and $n = 6$, $P < 0.01$). The same letter indicates nonsignificant differences between means (Supplemental Table S6).

protein), lipid and Gln metabolism (e.g. 3-hydroxyacyl-CoA dehydrogenase, Gln synthetase), and autophagy-related proteins 3 and 8D, ThiF family domain-containing protein, all of which were up-regulated during DILS. Concomitant with up-regulation of these genes was the intense down-regulation of genes involved in protein repair (putative Deg protease homolog), carbon fixation, and photosynthesis “light and dark” reactions (Fig. 6; Supplemental Table S4). Cluster D group genes had pronounced up-regulation throughout DILS and include those involved in gibberellin signaling (gibberellin receptor *GID1L2*), lipid catabolic processes (patatin family phospholipase, mitochondrial precursor of acyl-coenzyme A dehydrogenase, and citrate synthase), RNA methylation (rRNA 2-O-methyltransferase fibrillar 2, RNA cap guanine-N2 methyltransferase domain-containing protein, rRNA large subunit methyltransferase J), Gln catabolic processes (aldehyde dehydrogenase, aminotransferase) and protein translation (e.g. 40S ribosomal protein S27a, eukaryotic peptide chain release factor subunit 1-1, eukaryotic translation initiation factor 5A). Lastly, cluster E genes were prominently down-regulated and include those involved in cytokinin-related signaling pathway (genes encoding proteins homologous to *OsRR4* and *OsRR10* type-A response regulators), photosynthetic electron transport chain (PSI subunit VII), photosynthesis dark and light reaction (ribulose-phosphate 3-epimerase and chlorophyll a/b-binding protein, respectively), chlorophyll biosynthesis magnesium-protoporphyrin IX monomethyl ester cyclase) and nitrogen utilization (NAD-dependent epimerase/dehydratase).

Microarray Analysis Reveals Specific Differences in Gene Medleys between DILS and Developmental Senescence

Beside the five distinct gene groupings of GO biological processes during incremental DILS in Figure 6 is a lane showing comparative changes that occur during barley “developmental senescence.” Quantitatively, many differences were apparent between DILS and developmental senescence, but qualitative differences were more apparent in genes grouped in clusters C and D than those others described in the previous section. The developmental senescence in barley was characterized by up-regulation of jasmonate biosynthesis processes (as seen by a 4-fold increase in the expression of 3-ketoacyl-CoA thiolase gene), auxin-activated signaling pathway (e.g. auxin response factor 19), carbohydrate metabolism (e.g. β -amylase, trehalose-6-phosphate synthase; Fig. 6; Supplemental Table S4, clusters C and D). Moreover, opposite gene expression profiles also provided a comparison between DILS and developmental senescence, for example, the genes involved in carbohydrate metabolic process (e.g. phosphoenolpyruvate carboxykinase or beta-amylase), proteolysis (e.g. ubiquitin-conjugated enzyme), and lipid catabolic process (e.g. phospholipase D) that were down-regulated during DILS are

actually up-regulated during developmental senescence (Fig. 6; Supplemental Table S4, cluster C). Interestingly, the opposite trend of gene activation during DILS and inhibition during developmental senescence was observed among genes involved in RNA methylation (e.g. RNA 2-O-methyltransferase fibrillarlin 2), carbohydrate metabolic process (e.g. Suc synthase, glyceraldehyde-3-phosphate dehydrogenase, and enolase), and proteolysis (e.g. vacuolar-processing enzyme precursor; Fig. 6; Supplemental Table S4, cluster D).

Reversal of Dark-Induced Barley Leaf Senescence: Photosynthetic Quantum Conversion Parameters and Leaf Nitrogen Status

It has been stated that the terminal, senescing stage of a plant cell may be reversed if the functions of the chloroplasts can be restored (van Doorn and Yoshimoto, 2010). To evaluate limits of senescence-reversal ability, we measured the photosynthetic quantum conversion parameters and nitrogen status in barley leaves that underwent light re-exposure after different periods of dark incubation (Fig. 7; Supplemental Table S6). During this process of re-exposure to light, it was apparent that the parameters such as F_v/F_m , F_v'/F_m' , qP, Chl. Flv and NBI that had gradually decreased during DILS started to recover, their activity increasing compared to the control level (Fig. 7; Supplemental Table S6). The Rfd and Φ PSII parameters were also restored but with a delay, increasing after day 5 of light re-exposure. It is noted here that this reversal occurred in samples exposed to darkness until day 7 but not beyond, with dark incubation lasting longer than 7 d, causing an irreversible decline in all the measured parameters.

DISCUSSION

We present a cascade of consecutive events that define the DILS phenomenon in barley. Our studies demonstrate that early barley DILS involves well-orchestrated physiological and cytological transformations associated with the cessation of photosynthesis, loss of chlorophyll, and disintegration of chloroplasts. This is followed by advanced DILS, which involves disruption of the nucleus, mitochondria, and chromatin condensation accompanied with nDNA fragmentation and enhanced expression of Cys proteases and autophagy proteins. Soon after the initiation of DILS, senescence (Rfd) and microautophagy markers predominated synchronously. Dynamic response of the Rfd parameter from the very beginning of dark incubation was found associated with the sudden drop in overall photosynthetic efficiency, making it a valuable indicator of dark-induced stress. Similarly, Φ PSII parameter indicated gradual changes from the beginning of the DILS process. Both these parameters are considered indicators of CO_2 net assimilation as their values are dependent not only on the potential PSII quantum

conversion capacity but also to a large extent on the actual efficiency of electron transport and photochemical reactions in the chloroplast (Fracheboud and Leipner, 2003; Baker and Oxborough, 2004; Lichtenthaler et al., 2005; Wong et al., 2014). Also, gibberellin and ethylene biosynthesis pathways predominated during DILS in contrast to hormonal signaling via jasmonic acid, which is pivotal in developmental senescence and was in fact down-regulated in barley during DILS.

The analysis of PSII quantum conversion capacity parameters, F_v/F_m , F_v'/F_m' , and qP, indicated that photosystem complexes remained active up to day 7 of DILS and declined thereafter as PSII degradation became irreversible. A sharp decrease in Chl:Flv ratio (NBI) on day 7 of DILS concurrently with a substantial decrease in Rubisco protein level indicates loss of leaf nitrogen-requiring compounds. As the levels of nitrogenous compounds decreased, the available C was likely utilized for the synthesis of leaf flavonoids (Flv), as previously known (Cartelat et al., 2005). However, it is noted that chloroplast-localized PSII-D1 (PSBA-encoded) protein level and PSII activity were more stable during this stage of DILS. The 2-fold decrease in chlorophyll level during this period suggests that chloroplast dismantling is asynchronous across the leaf area, leaving PSII core proteins still around. These observations indicate differential kinetics of chloroplast protein breakdown during the early events of DILS, which could be part of a stress-adaptation strategy, similar to what was suggested previously (Krupinska et al., 2012). Thus, some active photosystems during this phase would be favorable for photosynthetic ATP synthesis in senescing leaves. Such a scenario is supported by the DILS microarray data showing a robust ATP-dependent metabolism of amino acids, fatty acids, pigments, and hormones until DILS enters an advanced, irreversible phase. The temporal prevention of LHCII disassembly seems similar to "delayed" PSII deficiency observed in functional stay-green mutants (Hörtensteiner, 2009).

Morphological changes together with catabolic processes associated with chloroplast disintegration became more apparent during DILS progression beyond day 7. Disintegration of chloroplasts correlated with the degradation of Rubisco and PsbA-D1 proteins, down-regulation of Gln synthetase-Gln oxoglutarate aminotransferase cycle enzymes, and activation of chloroplast isocitrate dehydrogenase (apparently necessary for 2-oxoglutarate anabolic export). Malate dehydrogenase genes specific for the two cellular compartments were found down-regulated, indicating that both glyoxylic and citric acid cycles might be compromised as dark-induced senescence progressed. This inhibition, however, does not seem to preclude the function of glyoxylic acid cycle to supplement cytosolic gluconeogenesis, since the genes for the key enzymes—pyruvate phosphate dikinase, PPI phosphofructokinase, and phosphoenol pyruvate carboxykinase—are actually induced (Table S2). Catabolic processes early in DILS were associated with

up-regulation of genes encoding cysteine and aspartyl proteases, ubiquitination enzymes, Hsp70, cytosolic Gln synthetase (Gln-1-3 isoform of low affinity to ammonia), and Orn cycle enzymes (P5C dehydrogenase, arginase, acetyl-Orn transaminase; Supplemental Table S2). The up-regulation of these genes highlights their role in dark-induced remobilization of degraded nitrogen compounds. Also, lipid catabolism intensified from day 7 onwards of DILS, suggesting that lipid degradation may contribute to energy-gaining processes, involving succinate synthesis within glyoxysomes and export thereafter to mitochondria. Degradation processes linked with respiration intensified at day 10, as shown by up-regulation of genes involved in vesicle recycling (SNARE complex, vesicle-fusing ATPase, signalosome complex) and cytochrome P450 (endoplasmic reticulum-bound form, involved in the formation of chlorophyll catabolites).

Mitochondria-associated metabolism during DILS supports its relevance in the allocation of recycled carbon substrates originating from degraded proteins, lipids, and/or other cellular components. In this regard, structurally mitochondria had longer durability until late stages of DILS within the same timeframe as the activation of glyoxylate cycle. One of the symptoms of PCD in animal and human cells is the reduction of transmembrane potential and change in the permeability of mitochondrial membranes, which leads to the release of cytochrome c from the intermembrane space to the cytosol (Barja, 2004; Jazwinski, 2004; Braeckman et al., 2009). However, chloroplasts but not mitochondria (like in animal PCD) seem to play the regulatory role in Arabidopsis leaf senescence (Zapata et al., 2005). According to the latter, genes encoding chloroplast NADH dehydrogenase-like complex (*NDH*) present in most higher plants are responsible for chloroplastic control of leaf senescence. The dark-mediated down-regulation of barley *NDH* seen in this study was most intense at day 3 of DILS, affirming that chloroplast processes are the early targets of barley leaf senescence.

Changes in the internucleosomal fragmentation of DNA (nDNA) has been considered as an indicator characteristic of PCD progression (van Doorn et al., 2011). Despite the fact that the comet assay has become one of the standard methods for assessing DNA damage, its application in detecting apoptosis (or PCD) was considered to be ambiguous (Collins et al., 2008). Nonetheless, photomicrographs are known to show the apoptotic morphology of lymphocyte nuclei as a large comet head (Singh, 2000). Our comet assay data are similar to the images seen earlier (Singh, 2000), suggesting finer DNA degradation on day 3 and PCD on days 7 and 10 in barley DILS.

Autophagy was prominent at each stage of DILS, from the beginning to the terminal phase. Therefore, senescence and autophagy seem to occur synchronously in DILS. Microautophagy initiated soon after senescence induction. Turnover of macromolecules via selective autophagy may contribute to cell homeostasis,

nutrient recycling, and clearance of damaged structures during DILS. That autophagy may play a role in nitrogen remobilization during developmental senescence of barley has been discussed previously (Hollmann et al., 2014). However, the functional autophagy switches between cell survival and cell death are not yet clear, but it is possible that vacuolar-processing enzymes (*VPEs*) are mediators of the crosstalk between PCD and autophagy (Patel et al., 2006; Floyd et al., 2015; Wang et al., 2018). Ultrastructural cell-death symptoms were found associated with induced expression of macro-autophagy related genes: *ATGs*, *VPEs*, and those involved in vesicle recycling on day 10 of DILS. How plant cells regulate stress-induced senescence via autophagy is an open question.

Two Agilent microarray data sets of barley analyzed during developmental leaf senescence are known (Christiansen and Gregersen, 2014; Hollmann et al., 2014). In one, barley plants were greenhouse-grown under artificial illumination supplemented with daily sunlight to ensure a day/night cycle of 16/8 h (Christiansen and Gregersen, 2014), and in the second, senescing and nonsenescing flag leaves of field-grown barley plants that received either a standard or a high dose of N fertilizer were analyzed (Hollmann et al., 2014). We compared the DILS microarray data set to these developmental senescence (DLS) microarray data sets, selecting 750 genes from the field experiment (Supplemental Fig. S2; Supplemental Table S5) and 22,000 gene probes from the greenhouse experiment (Fig. 6; Supplemental Table S4). Many similarities were apparent in gene expression between DILS and the DLS. For instance, common to both is an increased involvement of genes encoding glyoxysomal citrate synthase and mitochondrial succinate dehydrogenase. It appears that the regulation of these organellar energy-gaining processes is required to substitute for chloroplastic ATP synthesis both in DILS and DLS. Also, down-regulation of malate dehydrogenase in the two cellular compartments is notable. This effect, shared in both modes of leaf senescence, is apparently related to the suppression of chloroplastic glyceraldehyde-3-phosphate dehydrogenase, which functions as a part of a starch-degradation pathway that supports malate for other organelles in unstressed cells (Foyer et al., 2011). The most evident differences in gene medleys between DILS and DLS appeared among hormone-activated signaling pathways, lipid catabolic processes, carbohydrate metabolic processes, low-affinity ammonia remobilization and RNA methylation.

Further, DILS and DLS differ in the involvement of enzymes associated with cytosolic carbohydrate metabolism and lipid catabolism, since increased expression of glycolytic glyceraldehyde-3-phosphate dehydrogenase and enolase was evident in DILS but not in DLS. The by-product of this pathway is phosphoenolpyruvate, which can be directed into gluconeogenesis, which is upregulated in DILS. Evidently, a key enzyme in this process, pyruvate phosphate dikinase, is downregulated during DLS. This is congruent with

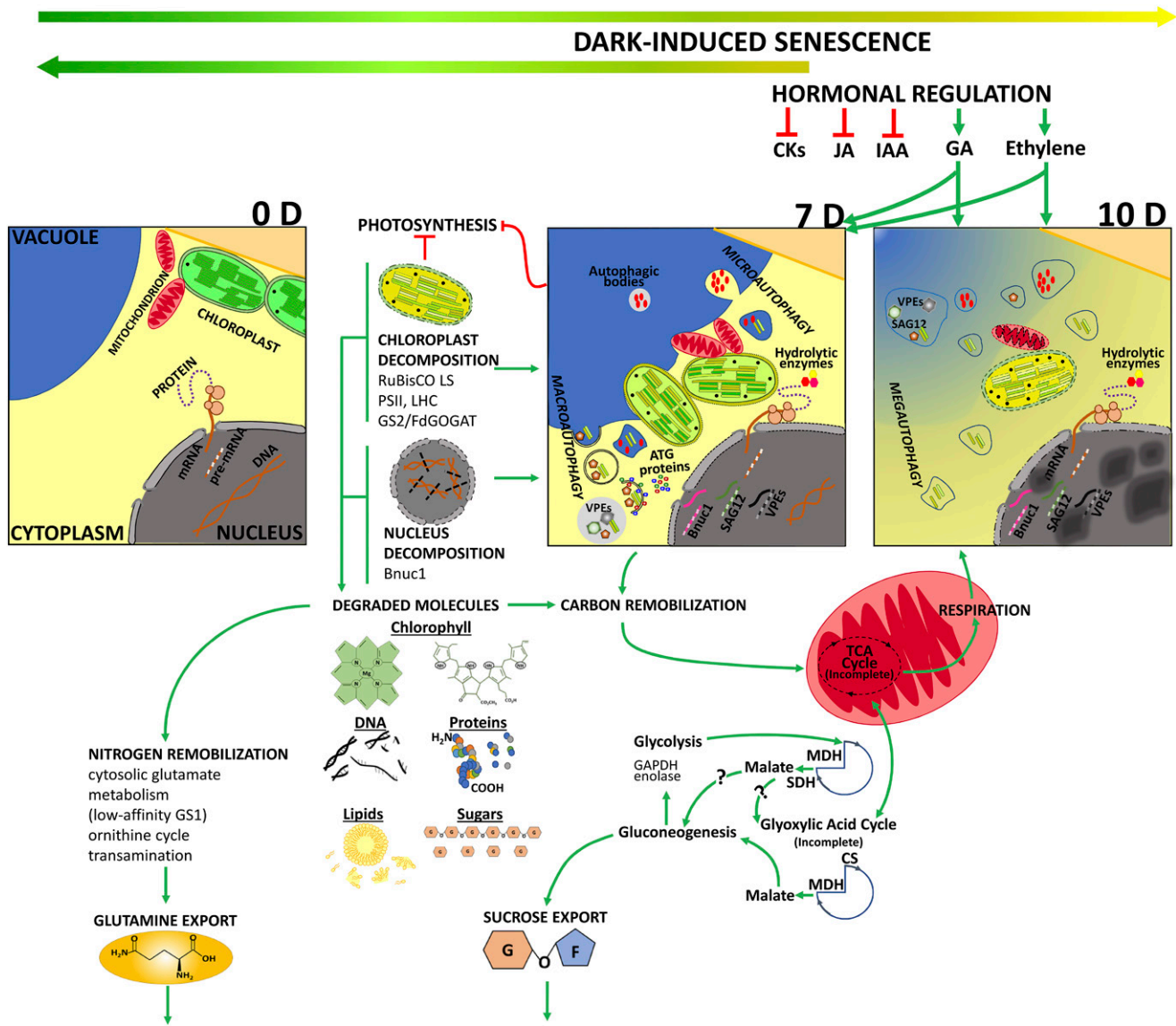


Figure 8. Dark-induced leaf senescence (DILS) model. Salient features of DILS in barley are summarized in the “Conclusion” section. The genes of gibberellin- and ethylene-mediated hormone signaling were up-regulated, whereas signaling involving the hormones jasmonic acid, auxin, and cytokinins was down-regulated in DILS. Earliest markers of barley DILS were loss of chlorophyll and decrease in photosynthesis. Chlorophyll fluorescence vitality index Rfd was the earliest parameter that correlated with the cessation of photosynthesis prior to microautophagy symptoms. Microautophagy began soon after senescence was induced, and all the organelles gradually disintegrated by day 10 of DILS, but the nucleus and mitochondria were relatively more stable until the final lytic stage. Ultrastructurally, cell death was associated with induced expression of autophagy-related, vacuolar-processing enzymes, and senescence-related genes. In spite of macro-autophagy, senescence reversal achieved by returning dark-incubated plants to the light (top backward arrow) was optimal/critical until the point of no return day 7 of DILS. Mitochondria and nuclei integrity seems related to the availability of recycled carbon substrates from degradation of proteins, lipids, and other organic cellular compounds. Increased expression of key genes of gluconeogenesis and glycolysis along with up-regulation of glyoxysomal enzymes are supportive of recycling of substrates.

enhancement of Suc synthase expression in DILS, whereas Suc export capacity was suppressed during DLS.

One of the other significant differences is in the lipid catabolism involving down-regulation of C- and D-type of phospholipase genes in DILS. Phospholipases are

well known to be involved in lipid catabolism as well as in GTP-dependent signaling pathway, interfering as effector proteins with α -subunit of G-protein-type receptors (Fukami, 2002; Jenkins and Frohman, 2005). Also of note is the fact that the gibberellin synthesis pathway is upregulated during DILS versus DLS,

while hormonal signaling via jasmonic acid and auxin appear to be pivotal for DLS.

In both the senescence models, low-affinity ammonia remobilization (cytosolic isoform of Gln synthetase 1 and Glu dehydrogenase) and Orn cycle transamination process were found activated. In comparison, branched-chained amino acid aminotransferases were upregulated during DILS but not DLS. The latter observation is consistent with the finding that enriched reserves of branched-chain amino acids are released during dark incubation of Arabidopsis leaves likely for the neutralization of toxic free ammonia from amino acids with high N:C ratios (Law et al., 2018). Finally, we also note here that the RNA methylation index was higher during DILS but not during DLS. This suggests the possibility of a yet-to-be discovered additional switch between cell survival and cell death.

Finally, day 7 of DILS was found to be the point of no return beyond which reversal of DILS did not occur. This was demonstrated by re-exposing the dark-incubated plants to light at different days during DILS. Barley plants in the dark up to day 7 were able to revert to efficient reconstruction of the Chl level that correlated with increased F_v/F_m , Φ PSII, and Rfd parameters. Beyond this stage, the nucleus and mitochondria that were otherwise stable until this point became susceptible to degradation, causing an irreversible decline. It is also noted here that for each of the indicators analyzed, a 2-d light re-exposure was insufficient to restore the level completely to that of the light control. This suggests that, in spite of the high capacity of chloroplasts to restore photochemical performance of converting solar energy (see also qP performance), the energy conversion of excitation and/or the use of potential energy, coupled with the transport of electrons, may be limited by some unknown factor whose reversibility is compromised. Thus, stress-induced leaf senescence in barley occurs in two phases. The first phase is more greatly emphasized by changes in chloroplast structure, photosynthesis function, proteins and specific gene medleys. The second, terminal phase, occurring beyond day 7, is characterized by irreversibility of senescence and its progression into PCD, exemplified by the involvement of both autophagy and PCD pathways.

CONCLUSION

In conclusion, the above findings are summarized diagrammatically in Figure 8. Regarding hormonal involvement, gibberellins and ethylene are particularly and positively associated with DILS in barley, while the jasmonic acid and cytokinin pathways were found down-regulated. Initiation of leaf senescence in DILS is marked by tonoplast invagination with fragmented cytosolic structures followed by rupturing of the vacuole and protoplast shrinking. Clearly, loss of chlorophyll, decrease in photosynthesis, and nuclear DNA fragmentation together with gradual disintegration

of chloroplast were prominent, while the nucleus and mitochondria were relatively more stable until the final lytic stage. Physically, cell death was concomitant with induced expression of senescence and autophagy-related and vacuolar-processing genes. In spite of advanced macro-autophagy, degradation processes were found to be reversible when plants at different stages of senescence were re-exposed to light until day 7. Day 7 of DILS was the point of no return when pigment loss, down-regulation of photosynthesis, and cell ultrastructure changes could not be reversed by re-exposure of plants to light. Remobilization of N was concurrent to up-regulation of cytosolic low-affinity Gln synthetase and Orn cycle enzymes. Chloroplast disintegration was accompanied by Gln synthetase-Gln oxoglutarate aminotransferase cycle inhibition and chloroplastic isocitrate dehydrogenase isoform activation, which may supplement mitochondrial catabolism with 2-oxoglutarate. The relatively more durable mitochondria appear to reutilize and recycle carbon substrates that likely originate from the degradation of proteins, lipids, and other organic cellular compounds. This conclusion is supported by increased expression of key genes of gluconeogenesis and glycolysis along with up-regulation of glyoxysomal citrate synthase and mitochondrial succinate dehydrogenase. Induction of Suc synthase suggests that up-regulation of the gluconeogenic pathway in darkness may be related to Suc export and/or malate recycling.

MATERIALS AND METHODS

Plant Material

Barley (*Hordeum vulgare*) seedlings were grown in growth chamber for 7 d on peat substrate for vegetables (1.0 kg/m³ NPK 14:16:18, neutralized by pH 5.5–6.0) under controlled conditions (day/night 16/8 h, 23°C, light intensity 150 μ mol m⁻² s⁻¹, 60% humidity). Pots with seedlings on seventh day of growth were transferred to dark conditions to initiate DILS after harvesting a few leaf samples for control. Thereafter, leaf samples from dark-induced seedlings were harvested on days 3, 7, and 10. For experiments that determined the optimal day(s) of darkness when the physiological recovery from senescence becomes irreversible, dark-incubated potted plants were selectively removed on days 3, 7, and 10 and returned to a photoperiod (day/night 16/8 h, 23°C, light intensity 150 μ mol m⁻² s⁻¹, 60% humidity) for 2, 5, and 7 d. The control plants were grown continuously under this photoperiod.

Measurement of Chlorophyll *a* Fluorescence Induction Kinetics

Chl fluorescence induction kinetics (the Kautsky effect) of nonstressed and dark-incubated barley plants were performed on leaf tissue (0.5-cm area, from 2–3 mm below the leaf tip) by using a pulse amplitude-modulated fluorimeter (FMS1, Hansatech) as described previously (Lichtenthaler et al., 2005). Predarkened leaves were analyzed for minimal fluorescence (F_0) upon exposure to weak far-red (735 nm) light pulses (5 s). After inducing fluorescence rise by high saturating light pulses (18,000 μ E m⁻² s⁻¹ for 2.5 s) to achieve maximum intensity level (F_m), the leaves were held for 2 min under white actinic light (180 μ E m⁻² s⁻¹, equivalent to irradiance used for acclimatization) for stable F value measurement. Then the minimum (F_0') and maximum (F_m') fluorescence level of the light-adapted state was determined in the same way as in the predarkened leaves (ETR, Φ PSII measurements). Alternatively, after F_m analysis, each leaf

was left for 3 to 5 min under continuous saturating light at $800 \mu\text{E m}^{-2} \text{s}^{-1}$, to avoid photoinhibition, for slow fluorescence decay (F_d) to attain a steady-state value (F_s) (Rfd measurement). In contrast to actinic light, high photon densities saturated the photosynthetic quantum conversion of nearly all leaf chloroplasts, and, therefore, Rfd measurement correlated well with overall net photosynthetic CO_2 -assimilation activity (Lichtenthaler et al., 2005). The *Chl* fluorescence kinetic parameters were calculated as follows:

Effective quantum yield of PSII electron transport, $\Phi\text{PSII} = (\text{Fm}'' - \text{F}) / \text{Fm}''$

Chl fluorescence decrease ratio, called vitality index, $\text{Rfd} = (\text{Fm} - \text{Fs}) / \text{Fs}$

Maximum quantum yield of PSII in the dark-adapted state, $\text{Fv} / \text{Fm} = (\text{Fm} - \text{F}_0) / \text{Fm}$

Maximum quantum yield of PSII in the light-adapted state, $\text{Fv}'' / \text{Fm}'' = (\text{Fm}'' - \text{F}_0'') / \text{Fm}''$

Photochemical quenching of Chl fluorescence, $\text{qP} = \text{Fm}'' - \text{F} / \text{Fm}'' - \text{F}_0''$

Non-photochemical quenching of Chl fluorescence, $\text{NPQ} = (\text{Fm} - \text{Fm}'') / \text{Fm}''$

Estimation of Leaf N Deficiency Progress

For nondestructive indication of leaf nitrogen deficiency progression, caused by dark-induced senescence, fluorimetry (DUALEX 4 Scientific FLAV fluorimeter; Force-A) was performed to estimate chlorophyll/flavonoid (Chl/Flv) ratio, called NBI, using a 0.5-cm area, 2 to 3 mm below the leaf tip. This nondestructive measurement is based on the idea that leaf N deficiency is associated with a decrease in fluorescence related to chlorophyll-protein complexes (Cartelat et al., 2005). The other indicator highly correlated with leaf N is total Flv content—the levels of these carbon-based metabolites increase under nutrient stress due to reduced use of carbon for N compound synthesis. Simultaneous fluorimetric measurement of Chl and Flv content in leaves allows for strong correlations with plant N management efficiency (Cerovic et al., 2002). The Flv level was estimated from the difference in chlorophyll fluorescence induced by UV (375 nm) and red light (650 nm), since only UV is affected by the presence of Flv. The chlorophyll level was estimated from red light (710 nm) transmittance. Since leaf structures could interfere with this measurement, the readings were automatically corrected by transmittance measured at the 850-nm reference wavelength (Cerovic et al., 2012).

Cytology-Related Analyses

For cytology experiments, control and senescent barley-leaf tissue (0.5-cm area, 2 to 3 mm below the leaf tip) were fixed immediately after harvest (excision) in 2% glutaraldehyde and 2% formaldehyde overnight with one change of solution at pH 6.8 (Polysciences). The fixed samples were rinsed three times with cacodylate buffer (0.05 M, pH 6.8; Polysciences), dehydrated in a graded ethanol series (10–100%), and postfixed with 1% osmium tetroxide for 2 h at room temperature. Fixed material was counterstained, embedded in low-viscosity resin, and processed as described previously (Bagniewska-Zadworna et al., 2012; Wojtyla et al., 2013). Ultrathin sections (0.1 μm) were cut with a diamond knife on an ultramicrotome EM UC6 (Leica-Reichert, Bensheim, Germany) and collected on Formvar-coated copper grids. The sections were examined with a JEM 1200 EX II transmission electron microscope (JEOL) operating at an accelerating voltage of 80 kV. From the same samples, semithin sections were collected and observed microscopically (the Zeiss LSM 510 model, Axiovert 200 M). At least five leaf fragments from each experimental variant were examined with an average of three copper grids per sample.

Chlorophyll Autofluorescence

Chlorophyll autofluorescence, excited with UV light, was observed using stereoscopic microscope (Stereo Lumar V12, equipped with a camera Asio CAM MRC5).

Comet Assay

DNA damage was determined by an alkaline comet assay as described previously (Olive and Banáth, 2006). Leaf samples (0.5-cm area, 2–3 mm below the leaf tip) were cut and chopped in 1 mL of ice-cold 0.2 M Tris (pH 7.5),

containing 4 mM MgCl_2 (6 H_2O) and 0.5% w/v Triton X-100 (Tris- MgCl_2 buffer). The nuclei were filtered through a 52- μm nylon net, sedimented by centrifugation at 200g for 5 min (4°C) in a swinging bucket rotor, and the pellet was resuspended in 200 μL of Tris- MgCl_2 buffer (Rucińska et al., 2004). The nuclei were then embedded in 0.5% low-melting-point agarose on glass slides. Following cell lysis, samples were treated with alkali (pH > 13) to unwind and denature the DNA and hydrolyze the damaged sites. Slides were washed first in 400 mM Tris, pH 7.5, then with water followed by 70% ethanol, and then dried at room temperature. Immediately and prior to scoring, the DNA was stained with 300 μL SYBR Green I (Molecular Probes Invitrogen; dilution 1:10,000). The comets were observed using a confocal fluorescence microscope (LSM 510 Carl Zeiss) equipped with an excitation filter of 500 to 550 nm and a barrier filter of 590 nm. The extent of DNA migration was determined using a CASP-image analysis system (University of Wrocław, Poland). The degree of DNA migration (a measure of possible DNA single-strand breaks, alkali-labile sites, and incomplete excision repair sites) was expressed as a percentage of DNA in tail. DNA head (DNAH) and DNA tail (DNAT) were measured as the sum of intensities of all points of the head and the tail, respectively. Percent tail DNA (%DNAT) was calculated as follows: %DNAT = $100\text{DNAT} / (\text{DNAH} + \text{DNAT})$. Nuclei for the comet assay were isolated from five leaves. Generally, 50 comets were scored from each treatment. The data from three experiments were pooled (150 comets) and the mean values ($\pm\text{SD}$ and $\pm\text{SE}$) were determined.

Microarray Data Analysis

The Barley Gene Expression Microarrays, $4 \times 44\text{K}$ plates (Agilent), were used to identify genes involved associated with DILS. The data discussed in this publication are deposited in the Gene Expression Omnibus (accession no. GSE62539). The microarray experiment (cRNA synthesis, hybridization, data collection and raw probe signal analysis) have been described previously (Zmienko et al., 2015a, 2015b). Each probe sequence was annotated as described previously (Dataset published 2014 via <https://doi.org/10.6084/m9.figshare.987111.v1>). F-test (ANOVA) was used to assess global differences between the different conditions. A moderate version of this test was applied to shrink the probe-wise sample variances to a common value and augment the degrees of freedom for the individual variances (Smyth, 2004). Thus, the F-statistic is an overall test computed from the set of t-statistics for a particular probe. All subsequent analyses were performed using probes with Benjamini-Hochberg-corrected moderated F-test P values below 0.0005. Log_2 fold-changes and Benjamini-Hochberg corrected P values were used for gene set enrichment analysis based on Gene Ontology (GO) terms (Ashburner et al., 2001). This analysis was performed using top GO library for R statistical language (Alexa and Rahnenfuhrer, 2010). In particular, two approaches were applied for this analysis—classic and weighed, both based on Fisher exact test calculations (Alexa et al., 2006).

To decipher the comprehensive DILS-related processes, we reanalyzed the microarray data obtained using developmentally senescing leaves (controls were the nonsenescing flag leaves harvested 5 d before anthesis, and the senescing leaves were harvested 30 d post anthesis—the selected barley leaves for analysis had ~50% green leaf area. For this, barley (*Hordeum vulgare*, cv Golden Promise) plants were grown in the greenhouse in pots containing a 50:50 peat:perlite mixture, and a standard nutrient solution was supplied via the irrigation system. Also, artificial illumination was used to supplement lack of sunlight to ensure a day/night cycle of 16/8 h, as described previously (Christiansen and Gregersen, 2014) (accession no. E-MTAB-2133). The gene expression profiles generated for developmentally senescing barley leaves described above were compared with the expression profiles of DILS. Hierarchical clustering and heat map were generated using the Genesis software (Sturn et al., 2002).

SDS-PAGE of Rubisco and D1 Immunoblotting

Plastids were isolated using differential centrifugation of whole-leaf homogenate as described previously (Sobieszczuk-Nowicka et al., 2008, 2015; Zmienko et al., 2015b). The intactness and purity of the isolated plastids were evaluated by phase-contrast microscopy, quantification of enzyme markers (Glu dehydrogenase, a mitochondrial marker enzyme; UDP-Glc pyrophosphorylase, cytosolic marker enzyme), and immunoblotting. Proteins from isolated chloroplasts were electrophoresed on SDS-PAGE using 14% acrylamide and 6 mM urea (Laemmli, 1970), and then electrotransferred onto PVDF mem-

branes (Roche Diagnostics). Primary anti-Rubisco and anti-PsbA-D1 protein (membrane-associated PSII reaction center D1 protein) antibodies (Agriseria AB) were used at 1:1,000 and 1:5,000 dilutions, respectively (Luciński et al., 2011; Grabsztunowicz et al., 2015). Horseradish peroxidase-conjugated goat anti-rabbit immunoglobulin G (Agriseria, AS09 605) was used as secondary antibody at 1:25,000 dilution. The relevant immunoreacted polypeptide bands were visualized using the ECL system (ECL) according to the manufacturer's recommendations (Lumi-Light western Blotting Substrate, Roche Diagnostics). The immunostained bands were quantified using the Gelix One 1d Software Version 4.1 (Biostep). The range of the linearity of immunoreaction was checked for each immunoblot. Data from protein blots showing linear relation between sample dilution and immunoreaction were used in the studies presented here.

Statistical Analysis

The differences in the measured parameters of chlorophyll *a* fluorescence and nitrogen status were statistically analyzed using one-way ANOVA and Tukey-Kramer Multiple Comparison post-hoc test. Means were considered as significantly different at $P < 0.01$. For the analysis of comet assay, Kruskal-Wallis ANOVA was used to determine statistical differences with nonparametric distribution, and statistical significance was set at $\alpha = 0.01$. The figures were created using the computer program Statistica (StatSoft).

Accession Numbers

The data were deposited in Gene Expression Omnibus repository and are accessible through GEO Series accession number GSE62539 (<http://www.ncbi.nlm.nih.gov/geo/query/acc.cgi?acc=GSE62539>; Barrett et al., 2011).

Supplemental Data

The following supplemental materials are available.

Supplemental Figure S1. Immunodetection of barley plastid Rubisco and membrane-associated photosystem II reaction center D1 protein during dark-induced leaves senescence.

Supplemental Figure S2. Hierarchical clustering of genes involved in dark-induced leaf senescence (DILS) and developmental leaf senescence (DLS).

Supplemental Table S1. Photosynthetic quantum conversion and leaf nitrogen status values in barley leaves undergoing dark-induced senescence.

Supplemental Table S2. A summary table of all barley DILS probes present on the Agilent Barley Microarray.

Supplemental Table S3. Data set that generated Figure 5: list of genes shown in the Venn diagram.

Supplemental Table S4. Data set that generated Figure 6: lists of genes belonging to each cluster.

Supplemental Table S5. Data set that generated Supplemental Figure S2: lists of genes belonging to each cluster.

Supplemental Table S6. Photosynthetic quantum conversion and leaf nitrogen status parameter values in barley leaves undergoing dark-induced senescence and regreening.

Received May 31, 2018; accepted July 15, 2018; published August 20, 2018.

LITERATURE CITED

- Alexa A, Rahnenführer J (2010) topGO: Enrichment analysis for Gene Ontology. <https://bioconductor.org/packages/release/bioc/html/topGO.html>
- Alexa A, Rahnenführer J, Lengauer T (2006) Improved scoring of functional groups from gene expression data by decorrelating GO graph structure. *Bioinformatics* 22: 1600–1607
- Ashburner M, Ball CA, Blake JA, Butler H, Cherry JM, Eppig JT, Harris M, Hill DP, Mungall C, Reiser L; Gene Ontology Consortium (2001) Creating the gene ontology resource: design and implementation. *Genome Res* 11: 1425–1433
- Avila-Ospina L, Marmagne A, Talbot J, Krupinska K, Masclaux-Daubresse C (2015) The identification of new cytosolic glutamine synthetase and asparagine synthetase genes in barley (*Hordeum vulgare* L.), and their expression during leaf senescence. *J Exp Bot* 66: 2013–2026
- Bagniewska-Zadworna A, Byczyk J, Eissenstat DM, Oleksyn J, Zadworny M (2012) Avoiding transport bottlenecks in an expanding root system: xylem vessel development in fibrous and pioneer roots under field conditions. *Am J Bot* 99: 1417–1426
- Baker NR, Oxborough K (2004) Chlorophyll fluorescence as a probe of photosynthetic productivity. In GC Papageorgiou, Goivindjee, eds, *Chlorophyll a Fluorescence: a Signature of Photosynthesis*. Springer Netherlands, Dordrecht, the Netherlands, pp 65–82
- Barja G (2004) Free radicals and aging. *Trends Neurosci* 27: 595–600
- Barrett T, Troup DB, Wilhite SE, Ledoux P, Evangelista C, Kim IF, Tomaszewski M, Marshall KA, Phillippy KH, Sherman PM, (2011) NCBI GEO: archive for functional genomics data sets—10 years on. *Nucleic Acids Res* 39: D1005–D1010
- Bassham DC, Laporte M, Marty F, Moriyasu Y, Ohsumi Y, Olsen LJ, Yoshimoto K (2006) Autophagy in development and stress responses of plants. *Autophagy* 2: 2–11
- Benjamini Y, Hochberg Y (1995) Controlling the false discovery rate: a practical and powerful approach to multiple testing. *J R Statist Soc B* 57: 289–300
- Bollhöner B, Prestele J, Tuominen H (2012) Xylem cell death: emerging understanding of regulation and function. *J Exp Bot* 63: 1081–1094
- Braeckman BP, Houthoofd K, Vanfleteren JR (2009) Intermediary metabolism. *WormBook February* 16: 10.1895/wormbook.1.146.1
- Breeze E, Harrison E, McHattie S, Hughes L, Hickman R, Hill C, Kiddle S, Kim YS, Penfold CA, Jenkins D, (2011) High-resolution temporal profiling of transcripts during Arabidopsis leaf senescence reveals a distinct chronology of processes and regulation. *Plant Cell* 23: 873–894
- Buchanan-Wollaston V, Earl S, Harrison E, Mathas E, Navabpour S, Page T, Pink D (2003) The molecular analysis of leaf senescence—a genomics approach. *Plant Biotechnol J* 1: 3–22
- Buchanan-Wollaston V, Page T, Harrison E, Breeze E, Lim PO, Nam HG, Lin JF, Wu SH, Swidzinski J, Ishizaki K, (2005) Comparative transcriptome analysis reveals significant differences in gene expression and signalling pathways between developmental and dark/starvation-induced senescence in Arabidopsis. *Plant J* 42: 567–585
- Cartelat A, Cerovic ZG, Goulas Y, Meyer S, Lelarge C, Prioul JL, Barbottin A, Jeuffroy MH, Gate P, Agati G, (2005) Optically assessed contents of leaf polyphenolics and chlorophyll as indicators of nitrogen deficiency in wheat (*Triticum aestivum* L.). *Field Crops Res* 91: 35–49
- Cerovic ZG, Ounis A, Cartelat A, Latouche G, Goulas Y, Meyer S, Moya I (2002) The use of chlorophyll fluorescence excitation spectra for the non-destructive in situ assessment of UV-absorbing compounds in leaves. *Plant Cell Environ* 25: 1663–1676
- Cerovic ZG, Masdoumier G, Ghozlen NB, Latouche G (2012) A new optical leaf-clip meter for simultaneous non-destructive assessment of leaf chlorophyll and epidermal flavonoids. *Physiol Plant* 146: 251–260
- Christiansen MW, Gregersen PL (2014) Members of the barley NAC transcription factor gene family show differential co-regulation with senescence-associated genes during senescence of flag leaves. *J Exp Bot* 65: 4009–4022
- Collins AR, Oscoz AA, Brunborg G, Gaivão I, Giovannelli L, Kruszewski M, Smith CC, Štětina R (2008) The comet assay: topical issues. *Mutagenesis* 23: 143–151
- El Hafid R, Smith DH, Karrou M, Samir K (1998) Physiological responses of spring durum wheat cultivars to early-season drought in a Mediterranean environment. *Ann Bot* 81: 363–370
- Floyd BE, Pu Y, Soto-Burgos J, Bassham DC (2015) To Live or Die: Autophagy in Plants. In AN Gunawardena and PF McCabe, eds, *Plant Program: Cell Death*. Springer International Publishing, Cham, Switzerland, pp 269–300
- Foyer CH, Noctor G, Hodges M (2011) Respiration and nitrogen assimilation: targeting mitochondria-associated metabolism as a means to enhance nitrogen use efficiency. *J Exp Bot* 62: 1467–1482
- Fracheoud Y, Leipner J (2003) The Application of Chlorophyll Fluorescence to Study Light, Temperature, and Drought Stress. In JR DeEll and PMA Toivonen, eds, *Practical Applications of Chlorophyll Fluorescence in Plant Biology*. Springer, Boston, MA, pp 125–150
- Fukami K (2002) Structure, regulation, and function of phospholipase C isozymes. *J Biochem* 131: 293–299

- Gepstein S, Glick BR (2013) Strategies to ameliorate abiotic stress-induced plant senescence. *Plant Mol Biol* 82: 623–633
- Gepstein S, Sabeji G, Carp MJ, Hajouj T, Neshier MFO, Yariv I, Dor C, Bassani M (2003) Large-scale identification of leaf senescence-associated genes. *Plant J* 36: 629–642
- Grabsztunowicz M, Górski Z, Luciński R, Jackowski G (2015) A reversible decrease in ribulose 1,5-bisphosphate carboxylase/oxygenase carboxylation activity caused by the aggregation of the enzyme's large subunit is triggered in response to the exposure of moderate irradiance-grown plants to low irradiance. *Physiol Plant* 154: 591–608
- Gregersen PL, Holm PB, Krupinska K (2008) Leaf senescence and nutrient remobilisation in barley and wheat. *Plant Biol (Stuttg) (Suppl 1)* 10: 37–49
- Guo Y, Cai Z, Gan S (2004) Transcriptome of Arabidopsis leaf senescence. *Plant Cell Environ* 27: 521–549
- Hara-Nishimura I, Hatsugai N, Nakaune S, Kuroyanagi M, Nishimura M (2005) Vacuolar processing enzyme: an executor of plant cell death. *Curr Opin Plant Biol* 8: 404–408
- Hensel LL, Grbić V, Baumgarten DA, Bleecker AB (1993) Developmental and age-related processes that influence the longevity and senescence of photosynthetic tissues in Arabidopsis. *Plant Cell* 5: 553–564
- Hollmann J, Gregersen PL, Krupinska K (2014) Identification of predominant genes involved in regulation and execution of senescence-associated nitrogen remobilization in flag leaves of field grown barley. *J Exp Bot* 65: 3963–3973
- Hörtensteiner S (2009) Stay-green regulates chlorophyll and chlorophyll-binding protein degradation during senescence. *Trends Plant Sci* 14: 155–162
- Jazwinski SM (2004) Yeast replicative life span—the mitochondrial connection. *FEMS Yeast Res* 5: 119–125
- Jenkins GM, Frohman MA (2005) Phospholipase D: a lipid centric review. *Cell Mol Life Sci* 62: 2305–2316
- Jing HC, Hille J, Dijkwel PP (2003) Ageing in plants: conserved strategies and novel pathways. *Plant Biol* 5: 455–464
- Jukanti AK, Heidlebaugh NM, Parrott DL, Fischer IA, McInnerney K, Fischer AM (2008) Comparative transcriptome profiling of near-isogenic barley (*Hordeum vulgare*) lines differing in the allelic state of a major grain protein content locus identifies genes with possible roles in leaf senescence and nitrogen reallocation. *New Phytol* 177: 333–349
- Kleber-Janke T, Krupinska K (1997) Isolation of cDNA clones for genes showing enhanced expression in barley leaves during dark-induced senescence as well as during senescence under field conditions. *Planta* 203: 332–340
- Krupinska K, Mulisch M, Hollmann J, Tokarz K, Zschiesche W, Kage H, Humbeck K, Bilger W (2012) An alternative strategy of dismantling of the chloroplasts during leaf senescence observed in a high-yield variety of barley. *Physiol Plant* 144: 189–200
- Laemmli UK (1970) Cleavage of structural proteins during the assembly of the head of bacteriophage T4. *Nature* 227: 680–685
- Lamb CA, Yoshimori T, Tooze SA (2013) The autophagosome: origins unknown, biogenesis complex. *Nat Rev Mol Cell Biol* 14: 759–774
- Law SR, Chrobok D, Juvany M, Delhomme N, Lindén P, Brouwer B, Ahad A, Moritz T, Jansson S, Gardeström P (2018) Darkened leaves use different metabolic strategies for senescence and survival. *Plant Physiol* 177: 132–150
- Lee RH, Wang CH, Huang LT, Chen SC (2001) Leaf senescence in rice plants: cloning and characterization of senescence up-regulated genes. *J Exp Bot* 52: 1117–1121
- Legocka J, Sobieszczyk-Nowicka E, Wojtyła Ł, Samardakiewicz S (2015) Lead-stress induced changes in the content of free, thylakoid- and chromatin-bound polyamines, photosynthetic parameters and ultrastructure in greening barley leaves. *J Plant Physiol* 186–187: 15–24
- Lichtenthaler HK, Langsdorf G, Lenk S, Buschmann C (2005) Chlorophyll fluorescence imaging of photosynthetic activity with the flash-lamp fluorescence imaging system. *Photosynthetica* 43: 355–369
- Lin JF, Wu SH (2004) Molecular events in senescing Arabidopsis leaves. *Plant J* 39: 612–628
- Lohman KN, Gan S, John MC, Amasino RM (1994) Molecular analysis of natural leaf senescence in *Arabidopsis thaliana*. *Physiol Plant* 92: 322–328
- Luciński R, Misztal L, Samardakiewicz S, Jackowski G (2011) Involvement of Deg5 protease in wounding-related disposal of PsbF apoprotein. *Plant Physiol Biochem* 49: 311–320
- Lutts S, Kinet JM, Bouharmont J (1996) NaCl-induced senescence in leaves of rice (*Oryza sativa* L.) cultivars differing in salinity resistance. *Ann Bot* 78: 389–398
- Mattoo AK, Handa AK (2003) Ethylene signaling in plant cell death. In LD Noodén, ed, *Plant Cell Death Processes*. Academic Press, San Diego, CA, pp 125–142
- Mattoo AK, Marder JB, Edelman M (1989) Dynamics of the photosystem II reaction center. *Cell* 56: 241–246
- Miersch I, Heise J, Zelmer I, Humbeck K (2000) Differential degradation of the photosynthetic apparatus during leaf senescence in barley (*Hordeum vulgare* L.). *Plant Biol* 2: 618–623
- Nam HG (1997) The molecular genetic analysis of leaf senescence. *Curr Opin Biotechnol* 8: 200–207
- Olive PL, Banáth JP (2006) The comet assay: a method to measure DNA damage in individual cells. *Nat Protoc* 1: 23–29 17406208
- Patel S, Caplan J, Dinesh-Kumar SP (2006) Autophagy in the control of programmed cell death. *Curr Opin Plant Biol* 9: 391–396
- Pic E, de La Serve BT, Tardieu F, Turc O (2002) Leaf senescence induced by mild water deficit follows the same sequence of macroscopic, biochemical, and molecular events as monocarpic senescence in pea. *Plant Physiol* 128: 236–246
- Rucińska R, Sobkowiak R, Gwóźdź EA (2004) Genotoxicity of lead in lupin root cells as evaluated by the comet assay. *Cell Mol Biol Lett* 9: 519–528
- Sakamoto W, Takami T (2014) Nucleases in higher plants and their possible involvement in DNA degradation during leaf senescence. *J Exp Bot* 65: 3835–3843
- Singh NP (2000) A simple method for accurate estimation of apoptotic cells. *Exp Cell Res* 256: 328–337
- Smart CM, Hosken SE, Thomas H, Greaves JA, Blair BG, Schuch W (1995) The timing of maize leaf senescence and characterisation of senescence-related cDNAs. *Physiol Plant* 93: 673–682
- Smyth GK (2004) Linear models and empirical bayes methods for assessing differential expression in microarray experiments. *Stat Appl Genet Mol Biol* 3: e3
- Sobieszczyk-Nowicka E, Krzesłowska M, Legocka J (2008) Transglutaminases and their substrates in kinetin-stimulated etioplast-to-chloroplast transformation in cucumber cotyledons. *Protoplasma* 233: 187–194
- Sobieszczyk-Nowicka E, Wieczorek P, Legocka J (2009) Kinetin affects the level of chloroplast polyamines and transglutaminase activity during senescence of barley leaves. *Acta Biochim Pol* 56: 255–259
- Sobieszczyk-Nowicka E, Zmienko A, Samelak-Czajka A, Łuczak M, Pietrowska-Borek M, Iorio R, Del Duca S, Figlerowicz M, Legocka J (2015) Dark-induced senescence of barley leaves involves activation of plastid transglutaminases. *Amino Acids* 47: 825–838
- Sobieszczyk-Nowicka E, Kubala S, Zmienko A, Małecka A, Legocka J (2016) From accumulation to degradation: reprogramming polyamine metabolism facilitates dark-induced senescence in barley leaf cells. *Front Plant Sci* 6: 1198
- Springer A, Acker G, Bartsch S, Bauerschmitt H, Reinbothe S, Reinbothe C (2015) Differences in gene expression between natural and artificially induced leaf senescence in barley. *J Plant Physiol* 176: 180–191
- Sturm A, Quackenbush J, Trajanoski Z (2002) Genesis: cluster analysis of microarray data. *Bioinformatics* 18: 207–208
- Thomas H (2013) Senescence, ageing and death of the whole plant. *New Phytol* 197: 696–711
- Uauy C, Distelfeld A, Fahima T, Blechl A, Dubcovsky J (2006) A NAC gene regulating senescence improves grain protein, zinc, and iron content in wheat. *Science* 314: 1298–1301
- van Doorn WG, Woltering EJ (2004) Senescence and programmed cell death: substance or semantics? *J Exp Bot* 55: 2147–2153
- van Doorn WG, Yoshimoto K (2010) Role of chloroplasts and other plastids in ageing and death of plants and animals: a tale of Vishnu and Shiva. *Ageing Res Rev* 9: 117–130
- van Doorn WG, Beers EP, Dangl JL, Franklin-Tong VE, Gallois P, Hara-Nishimura I, Jones AM, Kawai-Yamada M, Lam E, Mundy J (2011) Morphological classification of plant cell deaths. *Cell Death Differ* 18: 1241–1246
- Wang P, Mugume Y, Bassham DC (2018) New advances in autophagy in plants: regulation, selectivity and function. *Semin Cell Dev Biol* 80: 113–122
- Wehner GG, Balko CC, Enders MM, Humbeck KK, Ordon FF (2015) Identification of genomic regions involved in tolerance to drought stress and drought stress induced leaf senescence in juvenile barley. *BMC Plant Biol* 15: 125

- Wojciechowska N, Sobieszczuk-Nowicka E, Bagniewska-Zadworna A (2018) Plant organ senescence - regulation by manifold pathways. *Plant Biol (Stuttg)* **20**: 167–181
- Wojtyła Ł, Rucińska-Sobkowiak R, Kubala S, Garnczarska M (2013) Lupine embryo axes under salinity stress. I. Ultrastructural response. *Acta Physiol Plant* **35**: 2219–2228
- Wong S-L, Chen C-W, Huang M-Y, Weng J-H (2014) Relationship between photosynthetic CO₂ uptake rate and electron transport rate in two C₄ perennial grasses under different nitrogen fertilization, light and temperature conditions. *Acta Physiol Plant* **36**: 849–857
- Zapata JM, Guéra A, Esteban-Carrasco A, Martín M, Sabater B (2005) Chloroplasts regulate leaf senescence: delayed senescence in transgenic *ndhF*-defective tobacco. *Cell Death Differ* **12**: 1277–1284
- Zmienko A, Goralski M, Samelak-Czajka A, Sobieszczuk-Nowicka E, Figlerowicz M (2015a) Time course transcriptional profiling of senescing barley leaves. *Genom Data* **4**: 78–81
- Zmienko A, Samelak-Czajka A, Goralski M, Sobieszczuk-Nowicka E, Kozłowski P, Figlerowicz M (2015b) Selection of reference genes for qPCR- and ddPCR-based analyses of gene expression in senescing barley leaves. *PLoS One* **10**: e0118226